Ore Geology Reviews 81 (2017) 587–601

Contents lists available at ScienceDirect

Ore Geology Reviews

journal homepage: www.elsevier.com/locate/oregeorev

Genesis of the Kaladawan Fe–Mo ore field in Altyn, Xinjiang, China: Constraints from mineralogy and geochemistry

Cheng-Ming Wang [a,b], Li Zhang [a], Hao-Shu Tang [c,*], Hua-Yong Chen [a], Xi-Liang Li [d], Yi Zheng [e], Deng-Feng Li [a,b], Jing Fang [a,b], Lian-Hui Dong [d], Xun Qu [d]

[a] Key Laboratory of Metallogenic Dynamics, Guangzhou Institute of Geochemistry, Chinese Academy of Sciences, Guangzhou 510640, China
[b] University of Chinese Academy of Sciences, Beijing 100049, China
[c] State Key Laboratory of Ore Deposit Geochemistry, Institute of Geochemistry, Chinese Academy of Sciences, Guiyang 550081, China
[d] Xinjiang Bureau of Geology and Mineral Resources Exploration and Development, Urumqi 830000, China
[e] Guangdong Provincial Key Lab of Geological Processes and Mineral Resource Survey, Sun Yat-sen University, Guangzhou 510275, China

ARTICLE INFO

Article history:
Received 29 October 2015
Received in revised form 29 August 2016
Accepted 1 September 2016
Available online 4 September 2016

Keywords:
Kaladawan Fe–Mo ore field
Altyn Mountains
Magnetite geochemistry
Metallogeny
NW China

ABSTRACT

The Kaladawan Fe–Mo ore field in Altyn (Xinjiang Province, NW China) contains six Fe (–Mo) deposits, with total proven reserves of 60 Mt Fe and 10,000 t Mo. Tabular, lensoidal and stratiform orebodies occur in the Cambrian foliated marble, phyllite, carbonaceous slate, chlorite–sericite schist and quartz–sericite schist along the exocontact zone of the Kaladawan granite. Skarns are extensively developed and dominated by garnet, pyroxene, epidote, tremolite and actinolite, with minor chlorite, zoisite, quartz and calcite. Ore minerals are mainly magnetite and molybdenite. Five alteration and mineralization stages (I–V) were identified: the prograde (I) and retrograde (II) skarns are characterized by assemblages of garnet–pyroxene and epidote–tremolite–actinolite, respectively, intruded and replaced by mineral assemblages of magnetite–epidote–zoisite (III), quartz–sulfides (IV) and calcite–chlorite (V) in younging order. The Kaladawan garnet contains more andradite (61.2–94.4 mol%) than grossularite (37.5–5.0 mol%). Pyroxene is Mg-rich and Fe-poor, with an endmember range of 55.4–94.7 mol% diopside and 42.5–4.7 mol% hedenbergite. Amphibole comprises mainly tremolite and actinolite. The Kaladawan skarn mineral contents resemble typical skarn Fe and Mo deposits. In-situ LA-ICP-MS magnetite trace element analysis had identified unusually high Mg, Mo and Cr concentrations. The high Mo and the absence of molybdenite inclusions in magnetite suggest that the hydrothermal fluids may have been Mo-rich. The magnetite also contains similar (Ti + V) and (Al + Mn) values with typical skarn Fe deposits. Therefore, the Kaladawan Fe–Mo mineralization is best attributed to be skarn-type, and related to the Kaladawan granite intrusion.

1. Introduction

The Kaladawan Fe–Mo ore field is located in the newly-discovered Kaladawan Fe–Cu–Pb–Zn Polymetallic Metallogenic Belt in eastern Altyn Mountains, NW China (Fig. 1). It was discovered by the No. 1 Geological Party of the Xinjiang Bureau of Geology and Mineral Resources Exploration and Development (No. 1 XBGMRED) in 2006. The proven metal reserves of the ore field are 60 Mt Fe (average grade: 31.9%) with 10,000 t Mo as by product (XBGMRED, 2012). The Kaladawan Fe–Mo ore field contains five Fe deposits (i.e., Babaxi, Baba, 7914, 7915 and 7918) and one Fe–Mo deposit (i.e., 7910) (Fig. 1B and C, XBGMRED, 2012). These deposits share similar geological features, such as: 1) Stratiform (and also stratoid and lensoidal) orebodies hosted by Paleozoic volcanic–sedimentary sequences. 2) Spatial correlation between the Fe–Mo mineralization and skarn (garnet and actinolite) and/or potassic, silicic, chlorite, epidote and carbonate alterations. 3) The presence of numerous mafic to felsic plutons intruding in the Paleozoic sequences.

In the past, the Kaladawan Fe–Mo mineralization was variably attributed to "hydrothermal metasomatic-filling type" (Qi et al., 2008) or "synsedimentary–exhalative (SEDEX) type" (Chen et al., 2009, 2012; Gao et al., 2012; Hao, 2013). Recent studies attributed these deposits as typical submarine volcanogenic iron-oxide (SVIO) deposits, which were defined as volcanic-associated/volcanic-sedimentary-hosted Fe oxide deposits formed at or near the seafloor in submarine volcanic settings (Hou et al., 2014a; Zhang et al., 2014). However, limited information in the mineral assemblages and mineralization and alteration paragenesis has prevented conclusive characterization of the Kaladawan deposit type and metallogeny.

Magnetite, an important ore mineral in most Fe deposits, has long been used in deposit type fingerprinting and metal provenance studies

* Corresponding author.
E-mail address: tanghaoshu@163.com (H.-S. Tang).

http://dx.doi.org/10.1016/j.oregeorev.2016.09.001
0169-1368/

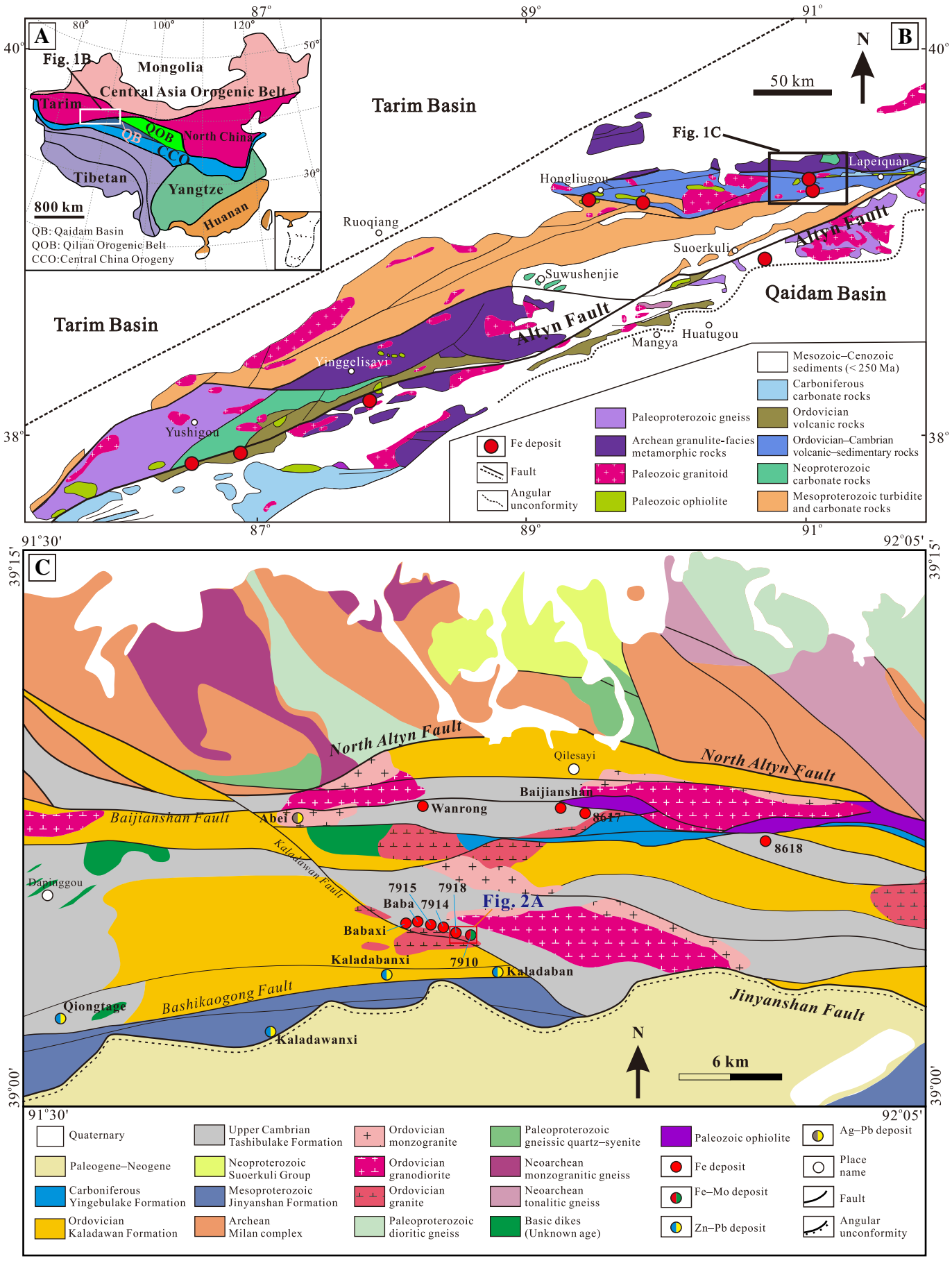
A
Fig. 1B
Mongolia
Central Asia Orogenic Belt
Tarim
QOB
QB
CCO
North China
Tibetan
Yangtze
Huanan
800 km
QB: Qaidam Basin
QOB: Qilian Orogenic Belt
CCO:Central China Orogeny
B
N
50 km
Tarim Basin
Fig. 1C
Lapeiquan
Hongliugou
Ruoqiang
Altyn Fault
Suoerkuli
Suwushenjie
Qaidam Basin
Tarim Basin
Mangya
Huatugou
Yinggelisayi
Yushigou
Mesozoic–Cenozoic sediments (< 250 Ma)
Carboniferous carbonate rocks
Ordovician volcanic rocks
Ordovician–Cambrian volcanic–sedimentary rocks
Neoproterozoic carbonate rocks
Mesoproterozoic turbidite and carbonate rocks
Paleoproterozoic gneiss
Archean granulite-facies metamorphic rocks
Paleozoic granitoid
Paleozoic ophiolite
Fe deposit
Fault
Angular unconformity
C
North Altyn Fault
Qilesayi
Baijianshan
Wanrong
Baijianshan Fault
Abei
8617
8618
Kaladawan Fault
Dapinggou
7915
7918
Baba
7914
Fig. 2A
Babaxi
Kaladabanxi
7910
Kaladaban
Qiongtage
Bashikaogong Fault
Jinyanshan Fault
Kaladawanxi
N
6 km
Quaternary
Paleogene–Neogene
Carboniferous Yingebulake Formation
Ordovician Kaladawan Formation
Upper Cambrian Tashibulake Formation
Neoproterozoic Suoerkuli Group
Mesoproterozoic Jinyanshan Formation
Archean Milan complex
Ordovician monzogranite
Ordovician granodiorite
Ordovician granite
Paleoproterozoic dioritic gneiss
Paleoproterozoic gneissic quartz–syenite
Neoarchean monzogranitic gneiss
Neoarchean tonalitic gneiss
Basic dikes (Unknown age)
Paleozoic ophiolite
Fe deposit
Fe–Mo deposit
Zn–Pb deposit
Ag–Pb deposit
Place name
Fault
Angular unconformity

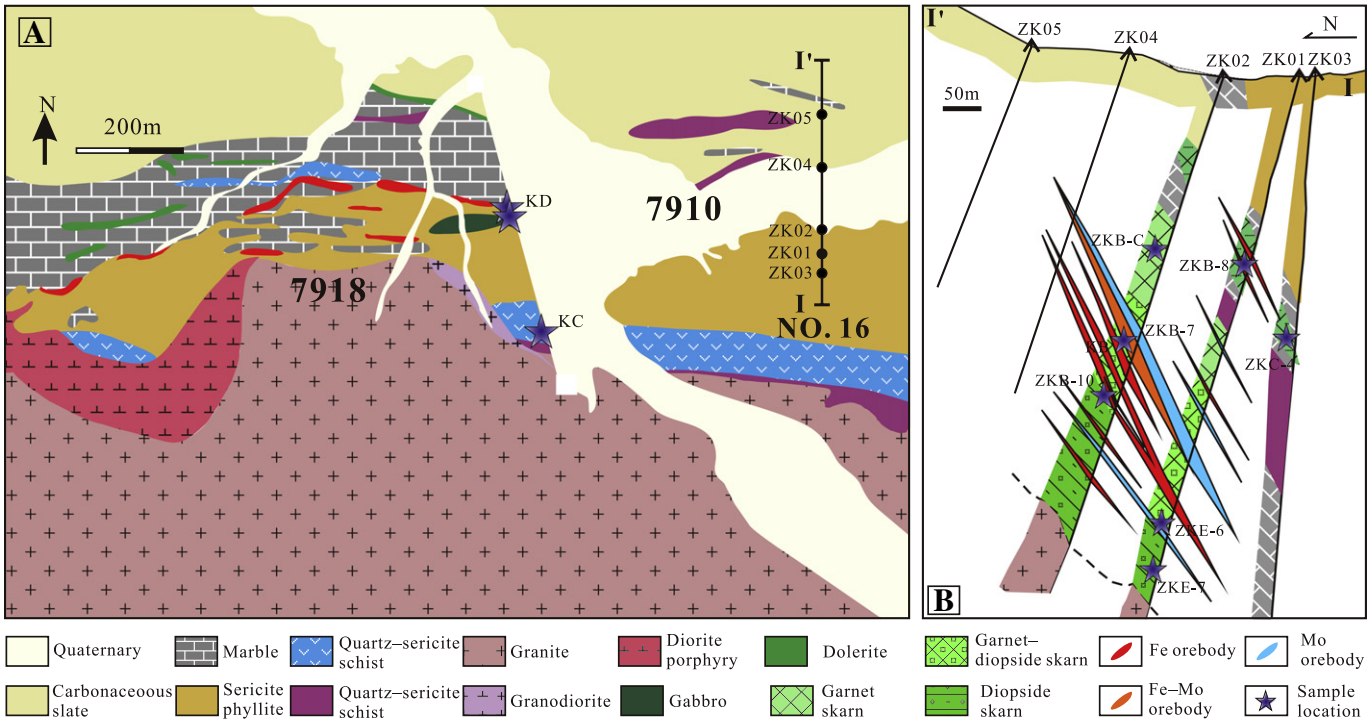

Fig. 2. (A) Geological map of the 7918 and 7910 deposits. (B) Geological cross section of the No. 16 prospecting line at the 7910 deposit, showing the orebody occurrence and its relationship with the intrusion and skarn.

(Ramdohr, 1926). This tool has become more powerful with the development of the LA-ICP-MS trace element analytical technology (e.g., Dare et al., 2014; Dupuis and Beaudoin, 2011; Nadoll et al., 2014a; Huang et al., 2015). In this paper, based on ore deposit geology, new obtained data on skarn mineralogy and in-situ LA-ICP-MS magnetite trace element geochemistry, we will identify the genesis of the Kaladawan Fe–Mo ore and discuss the relationship between the Fe and Mo mineralization and the metallogeny in this ore field.

2. Regional geology

The Altyn Mountains are located in the southeast of the Tarim Basin (NW China), and bordered with the Qaidam Basin along the Altyn Fault (Fig. 1A). The Kaladawan district is situated in the eastern Altyn Mountains (Fig. 1A, B). The basement of the district consists of the high-grade metamorphic Neoarchean Milan Complex, which is overlain by some sedimentary covers, i.e., the Proterozoic Jinyanshan Formation and Suoerkuli Group, Paleozoic Tashibulake and Kaladawan formations, and Cenozoic Yingebulake Formation (Fig. 1A and B). These stratigraphic units were folded into the Kaladawan Synclinorium (Hao, 2013).

The Milan Complex, bounded to the south by the EW-trending North Altyn Fault (Fig. 1C), is exposed in the northern Kaladawan district. The complex contains mainly granitic gneiss (resembling TTG rocks), K-feldspar–plagioclase gneiss, biotite–plagioclase gneiss (SHRIMP zircon U–Pb age: 2592 ± 15 Ma; Xin, 2012), hypersthene granulite and banded migmatite. As for the granitic gneiss, it is mainly composed of monzogranitic gneiss (SHRIMP zircon U–Pb age of 2830 ± 45 Ma), tonalitic gneiss (SHRIMP zircon U–Pb age: 2567 ± 38 Ma) and granodioritic gneiss (Xin, 2012). These Archean rocks were subjected to granulite-facies prograde metamorphism at ca. 2.40–2.35 Ga and amphibolite-facies retrograde metamorphism at ca. 2.0–1.9 Ga (Xin, 2012). Moreover, these metamorphic rocks were intruded by some Proterozoic plutons (later metamorphosed) (Xin et al., 2011), including plagioclase amphibolite (2374 ± 10 Ma), dioritic gneiss (2051.9 ± 9.9 Ma) and syenitic gneiss, with their protoliths being gabbro-dolerite, diorite and quartz syenite, respectively (Liu et al., 2009; Xin, 2012).

The Mesoproterozoic Jinyanshan Formation contains low-grade meta-carbonates intercalated with metamorphosed clastic rocks. The major rock types include crystalline/banded siliceous/stromatolite-bearing limestone, dolomite, foliated siltstone and silty mudstone, slate and phyllite with minor two-mica schist and mica–quartz schist (Hao, 2013). The formation was thrusted over the Miocene sequence along the Jinyanshan Fault (Fig. 1C). The Neoproterozoic Suoerkuli Group (northern Kaladawan) contains mainly dolomite, calcareous siltstone, oolitic chert, granule conglomerate, quartz sandstone and silty mudstone.

The Cambrian Tashibulake and Ordovician Kaladawan formations were juxtaposed over the Jinyanshan Formation by the Bashikaogong Fault (Fig. 1C). The Tashibulake Formation is the most important ore-bearing strata, hosting the Kaladawan Fe–Mo ore field and the Abei Ag–Pb deposit, and it has undergone greenschist-facies regional metamorphism. The formation contains meta-calcareous quartz sandstone, slate, sericite phyllite and minor two-mica–quartz schist and siliceous marble (XBGMRED, 2009). Fossil evidence (e.g., brachiopods: *Orthids* sp., *Finxelnburgia* sp. and *Xenorthis* sp.; Trilobites: *Yosimuraspis* sp. and *Lciosicglid* sp.) constrains the Tashibulake Formation to be the Late Cambrian (XBGMRED, 2009). And the Tashibulake Formation was intruded by Early Paleozoic granitoids (including diorite, granodiorite, monzogranite, granite) and minor gabbro–dolerite. The Kaladawan Formation contains mainly meta-basalt, meta-basaltic andesite, dacite, rhyolite, volcanic breccia, agglomerate and tuff (XBGMRED, 2009). The Yingebulake Formation is composed of limestone, sandstone and siltstone, exposed at Kaladawan locally (Cui et al., 2010). The Cenozoic sequence is mainly composed of conglomerate, sandstone and siltstone distributed in southern Kaladawan.

Fig. 1. (A) Tectonic framework of China, showing the location of the Altyn Mountains (modified after Li et al., 2012). (B) Geological map of the Altyn Mountains and the location of Kaladawan district (modified after He et al., 2005). (C) Local geology of the Kaladawan district, showing the location of the Kaladawan Fe–Mo ore field.

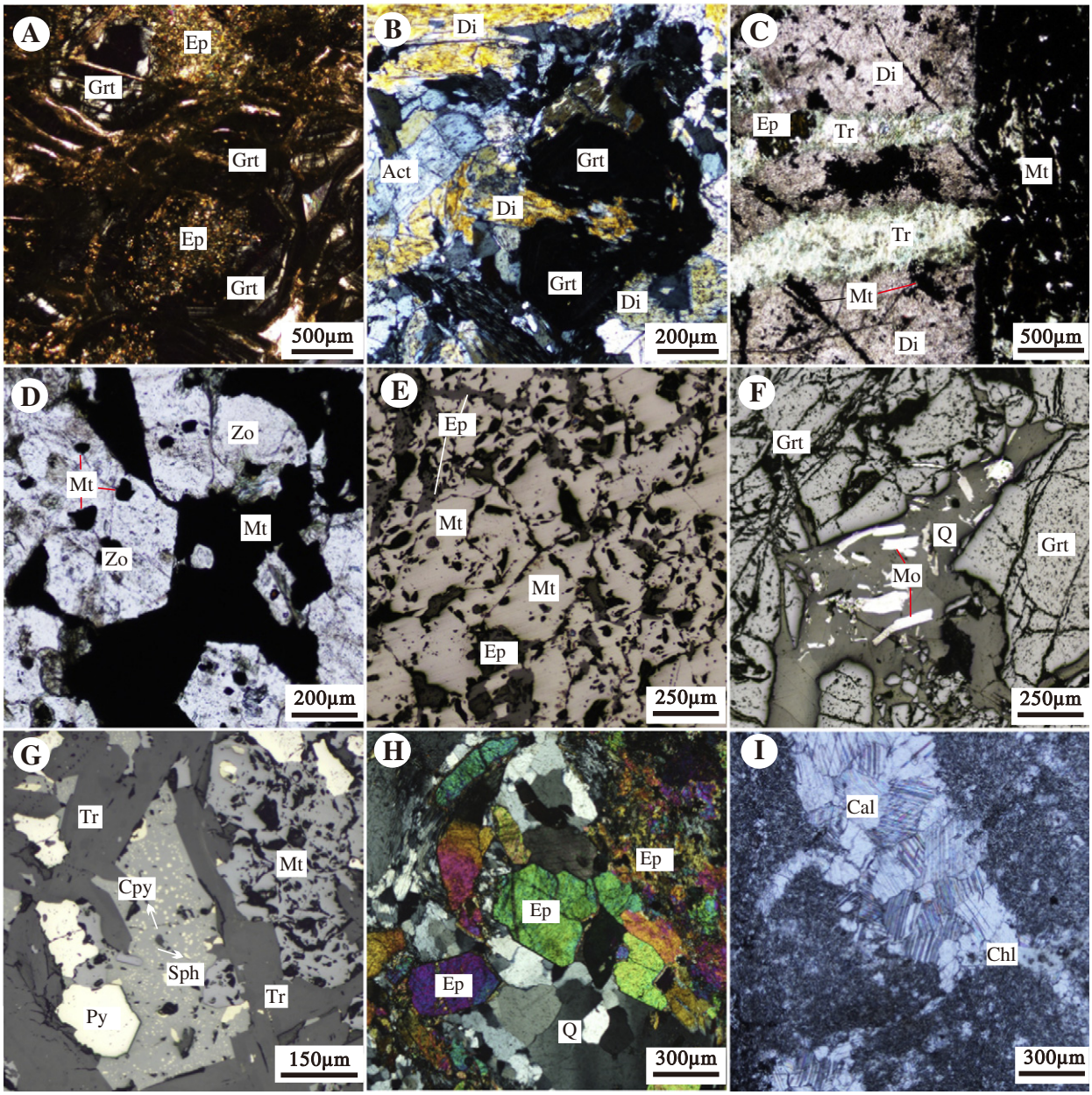

Fig. 3. Photomicrographs showing ore mineralogy and hydrothermal alteration and mineralization features. (A) *Type 1* garnet replaced by epidote and tremolite. (B) *Type 2* garnet intergrown with diopside. (C) Epidote–actinolite veins crosscutting diopside skarn, then crosscutted by magnetite–epidote vein. (D) Magnetite and zoisite. (E) Magnetite with epidote in massive ore. (F) Garnet filled by quartz–molybdenite ± calcite veinlets (reflected light). (G) Magnetite–actinolite assemblage replaced and filled by sphalerite–pyrite–chalcopyrite assemblage (reflected light). (H) Epidote replaced by quartz. (L) Calcite veinlets crosscutting dacite. Abbreviations: Grt, garnet; Di, diopside; Act, actinolite; Ep, epidote; Mt, magnetite; Q, quartz; Mo, molybdenite; Sph, sphalerite; Cpy, chalcopyrite; Py, pyrite; Cal, calcite.

Some ophiolitic segments are exposed in the east of the Kaladawan district and exhibit faulted contacts with the Paleozoic sequences. They consist mainly of peridotite, gabbro, sheeted dikes and basaltic lavas (Yang et al., 2008). Gabbro from the ophiolite has a zircon SHRIMP U–Pb age of 479.4 ± 8.5 Ma (Yang et al., 2008).

At least four major faults were identified in the Kaladawan district: 1) The oldest and largest North Altyn Fault (EW-trending and S-dipping) thrusted the Paleozoic sedimentary rocks over the Archean–Proterozoic metamorphic rocks and controlled the Paleozoic granitoid emplacements. 2) The younger Lapeiquan Normal Fault (EW-trending and S-dipping) was activated in ca. 220–180 Ma and reactivated in ca. 100 Ma (Chen et al., 2003). 3) The Jinyanshan Thrust Fault and its secondary faults, strike NEE, dip 45°–60° to the north and juxtaposed the Mesoproterozoic Jinyanshan Formation to the Cenozoic sedimentary sequence. 4) The youngest Kaladawan reverse faults may be linked to the sinistral shear along the Altyn Fault Zone (Fig. 1C).

The Kaladawan Fe–Mo field (including the Babaxi, Baba, 7914, 7915, 7918 and 7910 deposits) were developed in the Kaladawan district (Fig. 1C). This study focused on the 7918 and 7910 deposits in the Kaladawan field.

3. Deposit geology

The Kaladawan Fe–Mo ore field is located in the central Kaladawan district (Fig. 1C). Exposed strata include the Cambrian Tashibulake Formation foliated marble, sericite phyllite, carbonaceous slate, chlorite–sericite schist and quartz–sericite schist (Fig. 2, XBGMRED, 2012). The marble generally occurred as lenses in the chlorite schist and quartz–

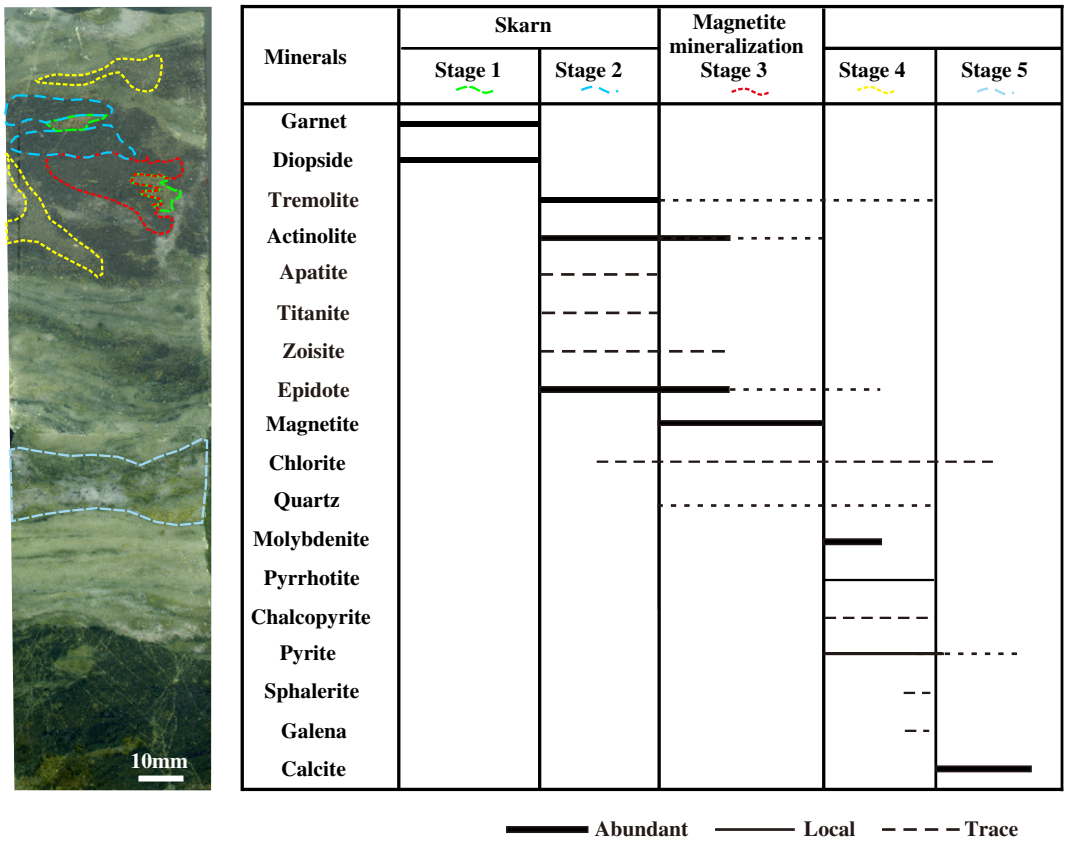

Fig. 4. Alteration and mineralization mineral paragenesis of the Kaladawan ore field.

chlorite–sericite schist. In the ore field, the Tashibulake Formation was intruded by gabbro and dolerite dikes, then intruded by the 476.1 ± 3.6 Ma Kaladawan granite (Wang et al., 2016). The Kaladawan granite was emplaced parallel to the North Altyn Fault (Fig. 1C) and was intruded by later granodiorite and diorite porphyry dikes and granite porphyry (Fig. 2A). The Kaladawan skarn alteration and mineralization occurred along the contact between the Kaladawan granite and the Tashibulake Formation. Alterations associated with the granite show a distinct zoning pattern from the granite outward: garnet + clinopyroxene skarns, to magnetite + molybdenite associated with epidote + actinolite ± tremolite skarns, to epidote + calcite ± wollastonite marble (Fig. 2B).

The orebodies strike 165°–212° and dip 50°–85° to the south, with Fe and Mo grades being 20.5–47.2% (average 31.86%) and 0.03–0.16% (average 0.07%), respectively. Magnetite is an important and abundant ore mineral. Other metallic minerals include molybdenite, pyrrhotite, pyrite, chalcopyrite, sphalerite, galena and scheelite. Gangue minerals include mainly garnet, diopside, tremolite, actinolite, epidote, zoisite, chlorite and calcite.

Most orebodies occur as lenses or veins in the exoskarn-altered wall rocks (Fig. 2B). Other alteration styles, including potassic, silicic, carbonate and chlorite alterations, were also identified. Hao (2013) reported individual molybdenite Re–Os ages ranging from 477.1 ± 7.0 Ma to 483.3 ± 7.0 Ma, with an isochron age of 480.2 ± 3.2 Ma, from the 7910 Fe–Mo deposit, later than its host rocks, i.e. the Tashibulake Formation.

4. Paragenesis of mineralization/alteration minerals

Five paragenetic stages (Stages I–V) were identified according to the mineral assemblages and their crosscutting relationship at the 7918 and 7910 deposits (Figs. 3 and 4).

I). Prograde skarn: The alteration was observed in both outcrops and drill cores. Massive skarn is well-developed along the intrusive contact between the Kaladawan granite and the Tashibulake Formation wall rocks, and contains mainly an mineral assemblage of garnet–pyroxene. Two types of garnet (*Type 1* and *2*) were identified: *Type 1* garnet (brownish-red to brown) is hypidiomorphic–idiomorphic, with medium- to coarse-grained blastic texture (Fig. 3A), mainly occurs in the volcanic wall rocks or hornfels around the granite, and is mostly anisotropic and exhibit anomalous optical characteristics and oscillatory zonation under plane-polarized transmitted light. *Type 2* garnet (yellowish-green to green) is idiomorphic, with medium- to coarse-grained blastic texture (Fig. 3B). Some *Type 2* garnet grains occur as intergrown with pyroxene along the contact with marble. Pyroxene mainly occurs as grayish-green fine-grained aggregates (Fig. 4B). Some pyroxenes also replaced garnets.

II). Retrograde skarn: The alteration is featured by an assemblage of amphibole (e.g., actinolite and tremolite) + epidote ± zoisite ± sphene ± apatite ± chlorite that crosscut or partially replaced garnet and pyroxene (Fig. 3B, C, D). Some amphiboles occur as columnar or fibrous and radiating aggregates (Fig. 3B), others (dark grayish-green) are with felted texture, filled in the fractures/fissures of the volcanic wall rocks or Stage I skarn, and intergrown with epidote grains (Fig. 3C). Epidotes occur as euhedral, coarse-grained crystals or fine-grained aggregates, and replaced garnets or hornblendes in the volcanic rocks (Fig. 4A). Some epidote grains partially replaced oscillatory-zoned garnets along its growth planes. Trace sphene and apatite occur along the granite–volcanic rocks intrusive contact.

III). Magnetite–epidote–zoisite: Retrograde alteration minerals were replaced by an mineral assemblage of magnetite + epidote ± amphibole ± zoisite. Some magnetite + epidote veins were

Table 1
EMPA data of diopside from the Kaladawan ore field.

Sample	ZKC-4-6	ZKC-4-3	ZKC-4-1	ZKB-7-7	ZKB-7-4	ZKB-7-8	ZKB-7-3	ZKE-7-3-	ZKB-7-2
SiO_2	53.04	52.78	54.01	52.62	53.94	54.25	52.76	52.35	54.34
TiO_2		0.06	0.01			0.01	0.02	0.05	
Al_2O_3	0.55	0.02	0.02	0.20	0.52	0.02	1.34	0.35	0.09
Cr_2O_3	0.03		0.01	0.02		0.02	0.01		
FeO	3.52	8.19	3.87	8.58	1.94	1.35	2.77	8.52	1.22
MnO	0.50	0.87	0.62	0.71	0.19	0.56	0.20	0.69	0.35
MgO	14.91	12.60	15.60	12.54	16.93	16.84	15.88	12.61	17.21
CaO	27.11	25.06	25.64	25.91	25.78	27.18	26.77	25.63	27.19
Na_2O	0.01		0.02	0.28	0.03	0.06	0.12	0.39	0.09
NiO									
K_2O	0.01	0.01	0.01		0.01		0.04	0.03	0.02
P_2O_5	0.03	0.04	0.02	0.04	0.06	0.04	0.02	0.02	0.04
BaO									
F									
Cl	0.15	0.11	0.10	0.10	0.12	0.08	0.06	0.04	0.08
Total	99.86	99.73	99.93	100.99	99.53	100.41	100.00	100.66	100.61
Number of ions on the basis of 6 atoms of oxygen									
Si	1.97	1.99	1.99	1.97	1.98	1.98	1.94	1.97	1.98
Al(IV)	0.00	0.00	0.00	0.00	0.02	0.00	0.06	0.00	0.00
Al(VI)	0.00	0.00	0.00	0.00	0.00	0.00	0.00	0.00	0.00
Ti	0.00	0.00	0.00	0.00	0.00	0.00	0.00	0.00	0.00
Cr	0.00	0.00	0.00	0.00	0.00	0.00	0.00	0.00	0.00
Fe^{3+}	0.06	0.02	0.02	0.10	0.03	0.07	0.10	0.12	0.08
Fe^{2+}	0.05	0.24	0.10	0.17	0.03	0.00	0.00	0.15	0.00
Mn	0.02	0.03	0.02	0.02	0.01	0.02	0.01	0.02	0.01
Mg	0.82	0.71	0.86	0.70	0.93	0.92	0.87	0.71	0.93
Ca	1.08	1.01	1.01	1.04	1.01	1.06	1.06	1.03	1.06
Na	0.00	0.00	0.00	0.02	0.00	0.00	0.01	0.03	0.01
K	0.00	0.00	0.00	0.00	0.00	0.00	0.00	0.00	0.00
Mn/Fe	0.17	0.11	0.16	0.08	0.10	0.27	0.06	0.08	0.14
Clinopyroxene components (mole fraction %)									
Jo	1.47	2.83	1.97	2.30	0.59	1.64	0.59	2.30	0.99
Hd	12.63	24.90	10.62	21.51	4.68	6.04	7.75	19.48	6.15
Di	85.90	72.27	87.41	76.19	94.73	92.32	91.66	78.22	92.86

Sample	ZKB-7-1	ZKB-C-6	ZKB-C-4	ZKB-C-3	ZKE-7-7	ZKE-6-2	ZKE-6-4	ZKE-6-1	ZKE-6-5
SiO_2	53.15	52.40	53.68	51.86	52.36	52.36	52.77	52.13	54.14
TiO_2				0.01	0.02	0.01		0.01	
Al_2O_3	0.57	0.05	0.09	0.04	0.26	0.04	0.34	0.25	0.08
Cr_2O_3				0.06			0.03	0.02	0.01
FeO	4.59	11.18	3.96	12.86	8.40	11.11	10.11	13.73	2.21
MnO	0.25	0.81	0.55	0.77	0.75	0.91	0.73	0.61	0.40
MgO	15.25	10.46	15.38	9.88	12.63	10.73	11.73	9.45	16.27
CaO	26.84	25.89	26.78	24.32	25.95	24.69	23.76	24.23	27.25
Na_2O	0.02	0.05	0.05	0.07	0.32	0.05	0.46	0.15	0.10
NiO						0.00		0.03	
K_2O	0.00			0.04		0.01		0.01	0.02
P_2O_5	0.02	0.05	0.03	0.01			0.02	0.03	0.05
BaO							0.02	0.00	
F									
Cl	0.03	0.05	0.04	0.12	0.01	0.01	0.01	0.01	
Total	100.73	100.93	100.56	100.03	100.70	99.92	99.96	100.66	100.52
Number of ions on the basis of 6 atoms of oxygen									
Si	1.96	1.99	1.98	1.99	1.97	2.00	2.00	1.99	1.98
Al(IV)	0.00	0.00	0.00	0.00	0.00	0.00	0.00	0.01	0.00
Al(VI)	0.00	0.00	0.00	0.00	0.00	0.00	0.01	0.00	0.00
Ti	0.00	0.00	0.00	0.00	0.00	0.00	0.00	0.00	0.00
Cr	0.00	0.00	0.00	0.00	0.00	0.00	0.00	0.00	0.00
Fe^{3+}	0.09	0.04	0.07	0.03	0.12	0.01	0.04	0.02	0.07
Fe^{2+}	0.05	0.31	0.05	0.39	0.14	0.34	0.28	0.42	0.00
Mn	0.01	0.03	0.02	0.03	0.02	0.03	0.02	0.02	0.01
Mg	0.84	0.59	0.84	0.57	0.71	0.61	0.66	0.54	0.89
Ca	1.06	1.05	1.06	1.00	1.04	1.01	0.96	0.99	1.07
Na	0.00	0.00	0.00	0.00	0.02	0.00	0.03	0.01	0.01
K	0.00	0.00	0.00	0.00	0.00	0.00	0.00	0.00	0.00
Mn/Fe	0.06	0.07	0.14	0.06	0.09	0.08	0.07	0.05	0.18
Clinopyroxene components (mole fraction %)									
Jo	0.74	2.54	1.68	2.62	2.44	3.04	2.73	2.11	1.19
Hd	11.99	34.91	10.70	39.31	19.90	34.65	26.23	42.54	6.86
Di	87.26	62.55	87.62	58.08	77.67	62.31	71.04	55.36	91.95

Jo—johannsenite, Hd—hedenbergite, Di—diopside.

Table 2
EMPA data of garnet from the Kaladawan ore field.

Sample	KC-1	KC-2	KC-3	KC-4	ZKB-C-1	ZKB-C-2	ZKB-C-2-	ZKE-7-7	ZKB-C-2--	ZKE-6-7	ZKE-6-2-	ZKB-C-5
Type	*Type 1*	*Type 1*	*Type 1*	*Type 1*	*Type 2*	*Type 2*	*Type 2*	*Type 2*	*Type 2*	*Type 2*	*Type 2*	*Type 2*
SiO_2	36.07	35.86	35.63	35.12	35.14	35.17	35.36	34.99	35.58	35.11	35.73	35.13
TiO_2						0.02	0.01			0.01	0.01	
Al_2O_3	2.99	2.85	1.93	0.52	0	0.14	0.64	0.9	0.22	0.87	1.66	0.71
Cr_2O_3		0.01	0.03	0					0.01		0.01	0.02
FeO_T	24.81	25	25.71	27.27	28.48	28.2	27.26	26.64	27.74	26.64	26.21	27.16
MnO	0.3	0.33	0.21	0.2	0.1	0.22	0.18	0.44	0.18	0.28	0.32	0.2
MgO	0.05	0.08	0.08	0.11	0.09	0.05	0.04	0.03	0.02	0.15	0.13	0.12
CaO	35.46	35.45	35.35	35.11	35.11	35.03	35.13	35.42	35.49	35.44	35.82	34.92
Na_2O	0.09	0.02	0.07	0.08	0.05			0.06	0.01	0.02	0.07	0
NiO									0.02	0.02		
K_2O	0.01	0	0	0.01			0.02		0.01			
P_2O_5	0.04	0.07	0.01	0.06	0.03	0.03	0.05	0.04	0.04	0.03	0.01	0.04
Cl	0.01	0.01	0	0.01	0.01	0	0.01	0	0.01	0	0.01	0
Total	99.82	99.67	99.04	98.48	99	98.87	98.69	98.52	99.33	98.55	99.97	98.3
Number of ions on the basis of 12 atoms of oxygen												
Si	2.95	2.94	2.95	2.94	2.93	2.94	2.95	2.93	2.95	2.93	2.93	2.94
Ti	0	0	0	0	0	0	0	0	0	0	0	0
Al	0.29	0.28	0.19	0.05	0	0.01	0.06	0.09	0.02	0.09	0.16	0.07
Cr	0	0	0	0	0	0	0	0	0	0	0	0
Fe^{3+}	1.7	1.71	1.78	1.91	1.99	1.97	1.9	1.86	1.93	1.86	1.8	1.9
Fe^{2+}	0	0	0	0	0	0	0	0	0	0	0	0
Mn	0.02	0.02	0.01	0.01	0.01	0.02	0.01	0.03	0.01	0.02	0.02	0.01
Mg	0.01	0.01	0.01	0.01	0.01	0.01	0	0	0	0.02	0.02	0.01
Ca	3.1	3.11	3.13	3.15	3.14	3.13	3.14	3.18	3.16	3.17	3.15	3.13
Garnet components (mole fraction %)												
Ura	0	0.04	0.09	0.01	0	0	0	0	0.02	0	0.03	0.06
And	81.21	81.73	84.47	90.14	94.41	93.59	90.35	87.09	91.06	86.98	84.67	90.26
Pyr	0.21	0.29	0.32	0.42	0.34	0.21	0.15	0.13	0.09	0.58	0.48	0.46
Spe	0.66	0.72	0.47	0.45	0.23	0.48	0.41	0.97	0.4	0.61	0.7	0.44
Gro	17.93	17.21	14.65	8.99	5.02	5.71	9.09	11.82	8.43	11.83	14.12	8.78
Alm	0	0	0	0	0	0	0	0	0	0	0	0
Other	0	0	0	0	0	0	0	0	0	0	0	0

Sample	ZKC-4-5	ZKC-4-3	ZKC-4-7	ZKC-4-2	ZKC-4-1	ZKB-7-6	ZKB-7-6-	ZKB-7-7	KB-1	KB-2	KB-3	KB-4
Type	Type 2	Type 2	Type 2	Type 2	Type 2	Type 2	Type 2	Type 2	Type 2	Type 2	Type 2	Type 2
SiO_2	36.67	34.89	35.05	36.16	35.42	34.68	34.01	35.03	34.93	35.23	34.19	34.21
TiO_2				0.01		0.06			0.18	0.2	0.04	
Al_2O_3	8.41	0.08	0.94	5	0.94	0.8	1.06	1.22	2.19	2.03	0.89	0.96
Cr_2O_3	0.01	0.01	0.04			0.02		0.09		0.01		
FeO_T	19.11	27.99	27.17	22.43	26.98	27.42	27.21	26.84	25.63	26.45	26.69	26.47
MnO	0.48	0.23	0.24	0.41	0.27	0.5	0.51	0.7	0.45	0.38	0.5	0.44
MgO	0.05	0.2	0.17	0.03	0.14	0.04	0.04	0.01	0.07	0.09	0.02	0.03
CaO	36.1	35.01	35.18	35.97	35.37	35.23	35	34.76	35.36	35.44	34.94	34.87
Na_2O	0.01	0.42	0.04	0.03	0.01	0.09	0.01	0.05	0.14	0.08	0.05	0.07
NiO												
K_2O	0.01	0.12				0.01		0.03	0.01	0.01		0.01
P_2O_5	0.03	0.06	0.04	0.05	0.05	0.04	0.04	0.05	0.05	0.03	0.04	0.03
Cl	0	0.01	0.01	0	0	0.01	0.01	0.01	0	0.01	0.01	0.01
Total	100.87	99.02	98.89	100.09	99.18	98.89	97.9	98.77	99.01	99.94	97.36	97.1
Number of ions on the basis of 12 atoms of oxygen												
Si	2.91	2.93	2.92	2.93	2.94	2.9	2.87	2.92	2.9	2.9	2.9	2.91
Ti	0	0	0	0	0	0	0	0	0.01	0.01	0	0
Al	0.79	0.01	0.09	0.48	0.09	0.08	0.11	0.12	0.21	0.2	0.09	0.1
Cr	0	0	0	0	0	0	0	0.01	0	0	0	0
Fe^{3+}	1.27	1.96	1.89	1.52	1.87	1.92	1.92	1.87	1.78	1.82	1.89	1.88
Fe^{2+}	0	0	0	0	0	0	0	0	0	0	0	0
Mn	0.03	0.02	0.02	0.03	0.02	0.04	0.04	0.05	0.03	0.03	0.04	0.03
Mg	0.01	0.03	0.02	0	0.02	0.01	0.01	0	0.01	0.01	0	0
Ca	3.07	3.15	3.14	3.12	3.14	3.16	3.17	3.11	3.15	3.12	3.18	3.18
Garnet components (mole fraction %)												
Ura	0.03	0.02	0.13	0	0	0.07	0	0.27	0	0.04	0	0
And	61.24	92.39	89.31	72.29	88.29	89.98	89.82	88.95	83.75	86.34	88.36	87.9
Pyr	0.17	0.78	0.67	0.11	0.54	0.16	0.16	0.03	0.29	0.35	0.06	0.11
Spe	1.03	0.51	0.54	0.89	0.59	1.11	1.13	1.57	0.99	0.83	1.12	0.98
Gro	37.53	6.29	9.35	26.7	10.58	8.67	8.88	9.18	14.97	12.43	10.45	11
Alm	0	0	0	0	0	0	0	0	0	0	0	0
Other	0	0	0	0	0	0	0	0	0	0	0	0

Ura—uvarovite, And—andradite, Pyr—pyrope, Spe—spessartine, Gro—grossularite, Alm—almandine.

Table 3
EMPA data of amphibole from the Kaladawan ore field.

Sample	ZKC-4-7	ZKC-4-2	ZKB-7-1	ZKB-10-1	ZKB-10-2-	ZKE-7-1	ZKE-7-1-	ZKE-7-3
SiO_2	54.20	54.46	53.60	57.18	57.26	53.68	54.38	54.39
TiO_2			0.04		0.03	0.02	0.02	0.03
Al_2O_3	0.54	0.74	0.86	0.02	0.05	0.75	1.93	2.27
Cr_2O_3	0.02			0.03		0.02		0.01
FeO	11.95	12.59	10.70	2.32	2.11	4.29	10.95	11.01
MnO	0.41	0.36	0.45	0.40	0.50	0.27	0.56	0.48
MgO	15.64	15.48	16.25	22.73	22.73	15.96	17.16	16.68
CaO	13.51	13.62	13.87	14.16	13.79	25.58	13.72	13.79
Na_2O	0.15	0.16	0.19	0.09	0.15	0.14	0.43	0.52
NiO								
K_2O	0.04	0.04	0.06	0.03	0.04	0.03	0.13	0.20
P_2O_5				0.03		0.07	0.02	0.02
BaO						0.03		
F								
Cl	0.09	0.12	0.14	0.07	0.07	0.04	0.01	0.06
Total	96.53	97.56	96.16	97.06	96.74	100.87	99.29	99.43
Number of ions on the basis of 23 atoms of oxygen								
Si	7.36	7.49	7.24	7.49	7.46	7.67	7.58	7.60
Al^{IV}	0.09	0.12	0.14	0.00	0.01	0.13	0.32	0.37
Al^{VI}	0.00	0.00	0.00	0.00	0.00	0.00	0.00	0.00
Ti	0.00	0.00	0.00	0.00	0.00	0.00	0.00	0.00
Fe^{3+}	0.00	0.00	0.00	0.00	0.00	0.51	0.35	0.44
Fe^{2+}	1.36	1.45	1.21	0.25	0.23	0.00	0.93	0.85
Mn	0.05	0.04	0.05	0.04	0.06	0.03	0.07	0.06
Mg	3.17	3.17	3.27	4.44	4.41	3.40	3.57	3.47
Ca	1.97	2.01	2.01	1.99	1.92	3.91	2.05	2.06
Na	0.04	0.04	0.05	0.02	0.04	0.04	0.12	0.14
K	0.01	0.01	0.01	0.00	0.01	0.01	0.02	0.04
Sum	14.03	14.34	13.98	14.24	14.13	15.70	15.00	15.03
OH^-	3.15	2.24	3.46	2.56	2.83	−0.83	0.66	0.53
F	0.00	0.00	0.00	0.00	0.00	0.00	0.00	0.00
Cl	0.00	0.00	0.00	0.00	0.00	0.00	0.00	0.00
Si_T	7.36	7.49	7.24	7.49	7.46	7.67	7.58	7.60
Al_T	0.09	0.12	0.14	0.00	0.01	0.13	0.32	0.37
Al_C	0.00	0.00	0.00	0.00	0.00	0.00	0.00	0.00
$Fe^{3+}{}_C$	0.00	0.00	0.00	0.00	0.00	0.51	0.35	0.44
Ti_C	0.00	0.00	0.00	0.00	0.00	0.00	0.00	0.00
Mg_C	3.17	3.17	3.27	4.44	4.41	3.40	3.57	3.47
$Fe^{2+}{}_C$	1.36	1.45	1.21	0.25	0.23	0.00	0.93	0.85
Mn_C	0.05	0.04	0.05	0.04	0.06	0.03	0.07	0.06
$Fe^{2+}{}_B$	0.00	0.00	0.00	0.00	0.00	0.00	0.00	0.00
Mn_B	0.00	0.00	0.00	0.00	0.00	0.00	0.00	0.00
Ca_B	1.97	2.00	2.00	1.99	1.92	2.00	2.00	2.00
Na_B	0.03	0.00	0.00	0.01	0.04	0.00	0.00	0.00
Ca_A	0.00	0.01	0.01	0.00	0.00	1.91	0.05	0.06
Na_A	0.01	0.04	0.05	0.01	0.04	0.04	0.12	0.14
K_A	0.01	0.01	0.01	0.00	0.01	0.01	0.02	0.04

Sample	ZKE-7-2	ZKE-6-2	ZKE-6-1	ZKE-6-5	KB-1-1	KB-1-2-	ZKB-2-1	ZKB-2-2
SiO_2	54.72	54.88	54.68	54.88	59.06	58.30	53.87	55.12
TiO_2	0.02		0.01	0.00	0.01	0.01	0.05	0.02
Al_2O_3	1.56	0.51	0.96	1.32	0.02	0.05	3.84	1.61
Cr_2O_3		0.03	0.00			0.00	0.05	0.01
FeO	10.08	12.90	12.67	11.90	1.66	2.37	9.55	9.71
MnO	0.51	0.47	0.45	0.40	0.33	0.66	0.24	0.28
MgO	17.26	15.76	15.73	16.11	23.78	23.02	16.97	17.72
CaO	13.71	13.74	13.75	13.91	14.17	13.83	13.49	13.85
Na_2O	0.38	0.18	0.22	0.24	0.04	0.03	0.51	0.09
NiO	0.02	0.00	0.04				0.01	0.01
K_2O	0.09	0.08	0.08	0.09	0.02	0.03	0.21	0.04
P_2O_5	0.01	0.02	0.02	0.01	0.02			0.01
BaO			0.03				0.03	0.02
F								
Cl	0.01	0.01	0.01		0.01	0.00	0.04	0.01
Total	98.36	98.59	98.65	98.85	99.11	98.30	98.83	98.48
Number of ions on the basis of 23 atoms of oxygen								
Si	7.52	7.65	7.62	7.63	7.83	7.70	7.42	7.55
Al^{IV}	0.25	0.08	0.16	0.22	0.00	0.01	0.58	0.26
Al^{VI}	0.00	0.00	0.00	0.00	0.00	0.00	0.04	0.00
Ti	0.00	0.00	0.00	0.00	0.00	0.00	0.01	0.00
Fe^{3+}	0.00	0.00	0.04	0.16	0.18	0.00	0.11	0.00
Fe^{2+}	1.16	1.50	1.44	1.22	0.00	0.26	0.99	1.11
Mn	0.06	0.06	0.05	0.05	0.04	0.07	0.03	0.03
Mg	3.53	3.28	3.27	3.34	4.70	4.53	3.48	3.62

Table 3 (*continued*)

Sample	ZKC-4-7	ZKC-4-2	ZKB-7-1	ZKB-10-1	ZKB-10-2-	ZKE-7-1	ZKE-7-1-	ZKE-7-3
Ca	2.02	2.05	2.05	2.07	2.01	1.96	1.99	2.03
Na	0.10	0.05	0.06	0.06	0.01	0.01	0.14	0.02
K	0.02	0.01	0.01	0.02	0.00	0.01	0.04	0.01
Sum	14.66	14.68	14.71	14.77	14.78	14.55	14.82	14.64
OH^-	1.50	1.31	1.26	1.07	0.78	1.50	1.07	1.39
F	0.00	0.00	0.00	0.00	0.00	0.00	0.00	0.00
Cl	0.00	0.00	0.00	0.00	0.00	0.00	0.00	0.00
Si_T	7.52	7.65	7.62	7.63	7.83	7.70	7.42	7.55
Al_T	0.25	0.08	0.16	0.22	0.00	0.01	0.58	0.26
Al_C	0.00	0.00	0.00	0.00	0.00	0.00	0.04	0.00
$Fe^{3+}{}_C$	0.00	0.00	0.04	0.16	0.18	0.00	0.11	0.00
Ti_C	0.00	0.00	0.00	0.00	0.00	0.00	0.01	0.00
Mg_C	3.53	3.28	3.27	3.34	4.70	4.53	3.48	3.62
$Fe^{2+}{}_C$	1.16	1.50	1.44	1.22	0.00	0.26	0.99	1.11
Mn_C	0.06	0.06	0.05	0.05	0.04	0.07	0.03	0.03
$Fe^{2+}{}_B$	0.00	0.00	0.00	0.00	0.00	0.00	0.00	0.00
Mn_B	0.00	0.00	0.00	0.00	0.00	0.00	0.00	0.00
Ca_B	2.00	2.00	2.00	2.00	2.00	1.96	1.99	2.00
Na_B	0.00	0.00	0.00	0.00	0.00	0.01	0.01	0.00
Ca_A	0.02	0.05	0.05	0.07	0.01	0.00	0.00	0.03
Na_A	0.10	0.05	0.06	0.06	0.01	0.01	0.13	0.02
KA	0.02	0.01	0.01	0.02	0.00	0.01	0.04	0.01

found crosscutting earlier skarn and amphibole veins (Fig. 3C). Magnetite mainly occurs as: (1) Euhedral to subhedral (0.1–3 mm) grains intergrown with zoisites (Fig. 3D); (2) Disseminated or massive aggregates coexisted with fine-grained green epidotes.

IV). Quartz–sulfides: Ore veins contain mainly molybdenite + quartz + calcite and minor pyrite + chalcopyrite + pyrrhotite + sphalerite + galena. Molybdenite grains appear either as disseminated bladed crystals in skarns, or as flake aggregates in quartz–calcite stockworks crosscutting the skarns (Fig. 3F). Tremolite and epidote were generally replaced by pyrite, sphalerite and chalcopyrite (Fig. 3G). Local pyrite occurs as idiomorphic and isolated crystals interstitial to garnet, pyroxene, amphibole and epidote.

V). Calcite–chlorite: Quartz and/or calcite veins and calcite–chlorite veins were extensively developed. Quartz veins commonly

Table 4
EMPA data of epidote from the Kaladawan ore field.

Sample	ZKC-4-6	ZKB-7-1	ZKB-7-1-	ZKE-7-1	ZKE-7-1-	ZKB-2-2	ZKB-2-3
SiO_2	36.79	37.05	37.18	37.80	37.59	38.58	38.67
TiO_2		0.11		0.04	0.12	0.08	0.05
Al_2O_3	21.80	22.77	22.68	22.61	22.86	28.32	28.42
Cr_2O_3		0.00	0.03	0.03	0.00	0.05	0.01
FeO	14.08	12.03	12.99	13.40	12.84	6.00	5.42
MnO	0.17	0.28	0.36	0.26	0.23	0.07	0.07
MgO	0.02	0.01	0.02		0.02	0.05	0.04
CaO	24.55	24.29	24.17	24.65	25.03	25.50	25.50
Na_2O	0.08	0.03	0.13	0.05	0.03	0.02	0.07
NiO				0.03			0.03
K_2O	0.01	0.02	0.04			0.02	0.04
P_2O_5	0.03	0.02	0.05	0.05	0.00	0.04	0.04
BaO					0.03		
F							
Cl	0.01	0.02	0.01	0.00	0.00	0.01	0.01
Total	97.53	96.63	97.65	98.91	98.76	98.73	98.35
Number of ions on the basis of 13 atoms of oxygen							
K	0.00	0.00	0.00	0.00	0.00	0.00	0.00
Ti	0.00	0.01	0.00	0.00	0.01	0.00	0.00
Na	0.01	0.00	0.02	0.01	0.00	0.00	0.01
W	0.00	0.00	0.00	0.00	0.00	0.00	0.00
Ca	2.10	2.09	2.06	2.07	2.11	2.10	2.11
Al	2.05	2.15	2.13	2.09	2.12	2.57	2.58
Sn	0.00	0.00	0.00	0.00	0.00	0.00	0.00
Fe^{3+}	0.94	0.81	0.86	0.88	0.84	0.39	0.35
Si	2.94	2.97	2.96	2.97	2.96	2.97	2.98
P	0.00	0.00	0.00	0.00	0.00	0.00	0.00
Mn	0.01	0.02	0.02	0.02	0.02	0.00	0.00
Mg	0.00	0.00	0.00	0.00	0.00	0.01	0.00
Mo	0.00	0.00	0.00	0.00	0.00	0.00	0.00
Total	8.07	8.05	8.06	8.04	8.06	8.05	8.05
Epidote components (mole fraction %)							
Piedmontite	0.01	0.02	0.02	0.02	0.02	0.00	0.00
Epidote	0.94	0.81	0.86	0.88	0.85	0.39	0.36
Clinozoisite	0.05	0.17	0.12	0.10	0.13	0.60	0.64

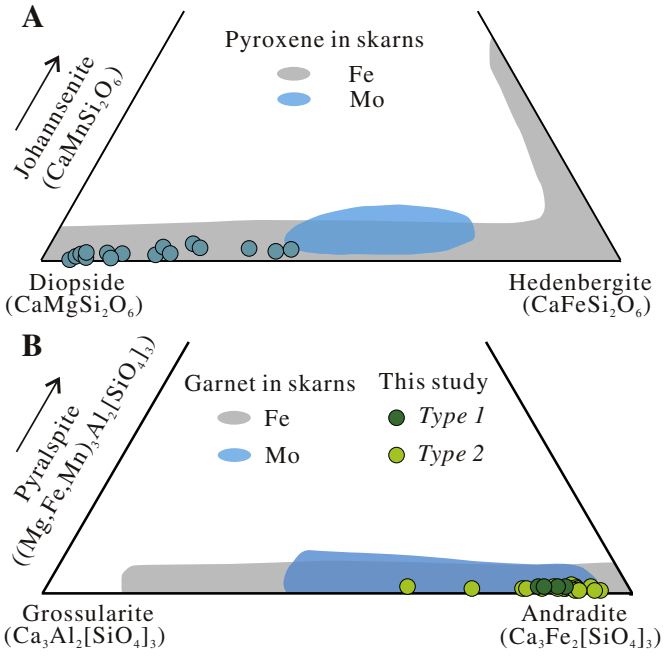

Fig. 5. (A) Ternary plot of pyroxene. (B) Ternary plot of the different garnet types. The fields for pyroxene and garnet from the skarn Fe and Mo deposits worldwide are from Meinert et al. (2005).

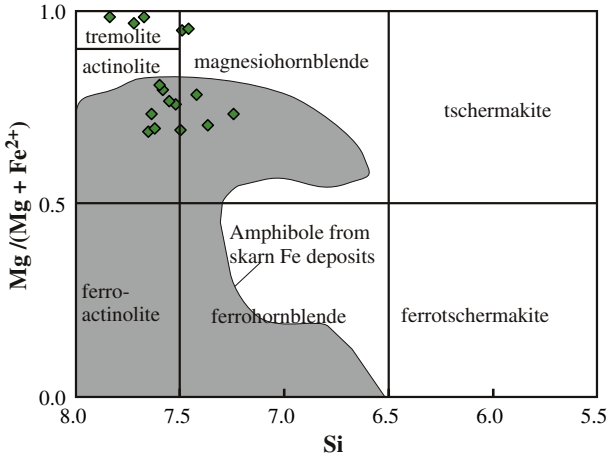

Fig. 7. Compositional classification of amphibole from the Kaladawan mineral district (after Leake et al., 2004). Compositional field of amphibole from Fe skarn deposits (Ettlinger, 1990; Pons et al., 2009; Sidder, 1985).

crosscut epidote (Fig. 3H). Many calcite–chlorite veins were found in the volcanic rocks distal to the granite intrusion (Fig. 3I).

Detailed alteration and mineralization paragenesis at Kaladawan was shown in Fig. 4.

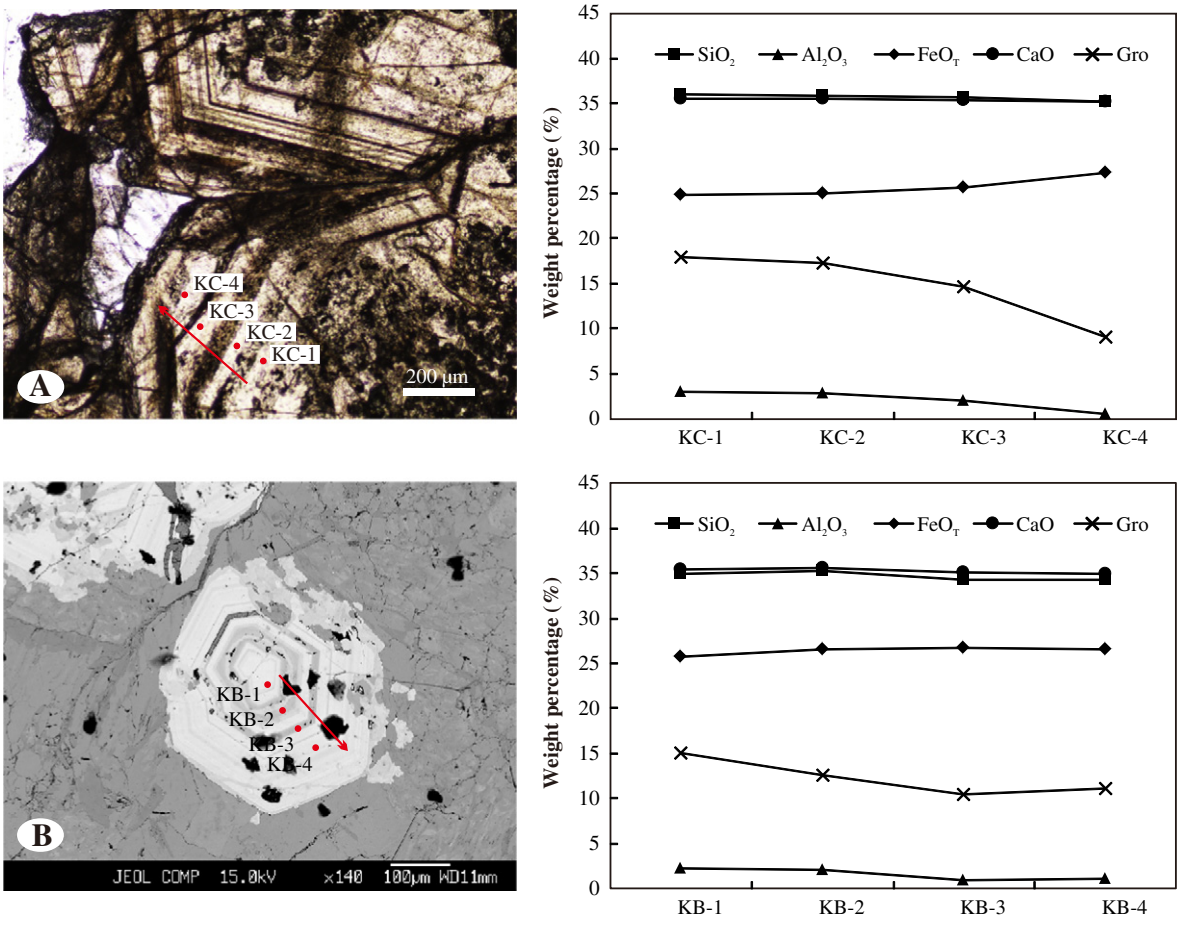

Fig. 6. Compositional changes from core to rim of zonal garnet. (A) Garnet from granite–volcanic rocks contact. (B) Garnet from the granite–marble contact.

Table 5
LA-ICP-MS results for trace elements in magnetite from the Kaladawan ore field.

Sample	MgO	Al_2O_3	SiO_2	P_2O_5	CaO	Sc	TiO_2	V	Cr	MnO	Co	Ni	Cu	Zn	Ga
	wt%	wt%	wt%	wt%	wt%	ppm	wt%	ppm	ppm	wt%	ppm	ppm	ppm	ppm	ppm
ZKB-7	0.00936	0.02446	0.07321	0.00784	0.02809	0.34543	0.00849	113.25339	<2.20053	0.09529	28.02322	12.24880	<1.088	40.05985	3.39043
ZKB-7	0.02032	0.03231	0.07570	0.00369	0.02162	0.10299	0.00937	94.05746	3.74079	0.10678	29.30482	13.21635	0.47349	42.04840	4.29008
ZKB-7	0.02723	0.02497	0.09642	0.00371	0.03923	0.08564	0.01673	177.38891	552.52344	0.07669	25.08815	21.79608	0.38420	28.55114	3.23829
ZKB-7	0.06664	0.03262	0.26753	0.00328	0.07472	0.14364	0.03081	147.96579	72.82243	0.08544	22.96771	18.48521	0.30871	22.37697	2.91815
ZKB-7	0.08393	0.04740	0.19408	0.00411	0.01864	0.15802	0.00977	108.63996	0.84127	0.10270	29.98381	14.92297	0.36377	44.74208	4.44462
ZKB-7	0.01800	0.02611	0.06626	0.00375	0.24604	0.12225	0.00981	132.76632	9.45293	0.10494	28.29583	17.14782	6.53638	57.98936	4.18967
ZKB-7	0.13178	0.06635	0.30977	0.00246	0.04743	0.55810	0.06418	132.03496	74.54446	0.10652	27.96130	17.24217	3.32711	56.63557	4.43180
ZKB-7	0.00826	0.02423	0.03812	0.00447	0.02212	0.12036	0.00815	131.91887	8.50084	0.10222	26.60076	18.88480	0.30947	52.13710	4.57209
ZKB-7 aver	0.04569	0.03481	0.14014	0.00328	0.10185	0.25470	0.01966	129.75321	120.26415	0.09757	27.27820	16.74302	4.93175	43.06756	3.93439
ZKB-10	1.10512	0.44254	1.15382	0.00911	0.13356	0.36417	0.04682	30.84206	32.38286	0.32307	0.21824	2.27016	0.76013	60.34114	2.15988
ZKB-10	0.53966	0.17281	0.53322	0.00276	0.02259	0.39550	0.04534	30.23216	32.24791	0.31539	0.24523	1.99403	2.64746	86.27385	1.57034
ZKB-10	1.95029	0.82791	1.73119	0.00316	0.05152	0.51034	0.04300	31.30779	28.21829	0.28680	0.12069	1.95500	0.38556	43.61094	2.14017
ZKB-10	0.29171	0.05861	0.37651	0.00252	0.22108	0.18713	0.06700	30.60159	863.22042	0.32987	0.27897	4.66677	1.73919	89.56753	1.75080
ZKB-10	4.37914	1.89062	3.91654	0.00436	0.02067	0.88064	0.08680	29.94519	165.03089	0.28033	0.21359	6.68878	3.39739	64.48950	3.09814
ZKB-10	0.52562	0.14795	0.46305	0.00414	0.03712	0.42825	0.06424	30.00430	3.79344	0.36602	0.15339	1.85049	0.31601	84.37494	1.51382
ZKB-10	1.41653	0.34136	1.50665	0.00329	0.05795	0.45546	0.03770	32.52777	15.13227	0.26736	0.23466	5.85087	11.74879	38.90662	1.66790
ZKB-10	0.48612	0.14692	0.41149	0.00298	0.02146	0.24398	0.08446	28.14029	2.22714	0.38957	0.29766	2.19825	0.60820	111.97909	1.56529
ZKB-10	0.54759	0.15189	0.52730	0.00355	0.02024	0.16311	0.04540	27.06150	4.79061	0.32359	0.18217	7.87246	1.07186	126.97660	2.10839
ZKB-10	1.57915	0.60628	1.58630	0.00507	0.03042	0.40449	0.04053	31.63931	90.64937	0.29574	0.23529	4.39682	11.24409	232.34607	1.80817
ZKB-10	0.96938	0.18266	0.98580	0.00787	0.03518	0.35662	0.04578	30.36626	27.27406	0.29004	0.22421	5.58912	0.85472	29.09164	1.82514
ZKB-10 aver	1.25366	0.45178	1.19926	0.00591	0.08712	0.49126	0.05519	30.24257	114.99702	0.31525	0.21796	4.12116	5.30813	87.99617	1.92800
ZKB-11	0.22478	0.03471	0.16236	0.00296	0.02166	0.27395	0.04802	24.56206	<1.3601	0.37996	15.68467	2.18896	0.30775	103.56101	1.44216
ZKB-11	0.27225	0.05523	0.20591	0.00370	0.01494	0.30382	0.04958	24.01464	<1.41723	0.33704	10.02226	2.34863	0.31185	111.45030	1.22548
ZKB-11	0.43448	0.15790	0.30430	0.00231	0.01564	0.28536	0.04365	22.26102	10.42806	0.31156	15.13191	2.47239	2.50896	118.22545	1.38366
ZKB-11	1.32303	0.54058	1.26130	0.00900	0.01880	0.33920	0.03598	23.67910	19.00168	0.24754	14.37932	2.45906	1.45418	83.89711	1.77851
ZKB-11	1.91048	0.85605	1.59940	0.00378	0.08729	0.46266	0.04346	23.91151	51.88491	0.33266	12.07859	1.94779	10.85511	122.29726	2.22936
ZKB-11	0.19581	0.02702	0.12206	0.00370	0.01754	0.19022	0.03884	24.06616	<1.90507	0.32584	10.24500	2.38779	0.50397	88.10697	1.87503
ZKB-11	0.13142	0.01550	0.10760	0.00386	0.01953	0.19152	0.04188	23.85059	<1.28404	0.31425	10.39315	2.02872	0.38455	62.56887	1.40878
ZKB-11	0.11198	0.01308	0.09243	0.00312	0.02565	0.16227	0.03765	23.27440	11.98654	0.29999	13.22358	1.65630	0.55875	73.96993	1.20784
ZKB-11	0.27633	0.03835	0.21911	0.00391	0.03040	0.31490	0.07083	24.39028	<1.21888	0.35488	1.89904	2.02580	0.42063	108.80966	1.64004
ZKB-11 aver	0.54229	0.19316	0.45272	0.00489	0.04258	0.28043	0.04554	23.77886	23.32530	0.32264	11.45084	2.16838	4.93942	96.98739	1.57676

Sample	Ge	As	Rb	Sr	Y	Zr	Nb	Mo	Ba	La	Ce	Pr	Nd	Sm	Eu
	ppm	ppm	ppm	ppm	ppm	ppm	ppm	ppm	ppm	ppm	ppm	ppm	ppm	ppm	ppm
ZKB-7	4.76052	0.81465	0.10790	0.03932	0.08851	0.08835	0.05677	2.25289	0.39701	0.03366	0.07069	0.03859	0.15533	0.04812	0.05034
ZKB-7	<1.86647	1.08300	0.06594	0.00000	0.00000	0.15399	0.04633	0.48274	0.55116	0.02217	0.02043	0.00000	0.12791	0.00000	0.04128
ZKB-7	2.06856	0.82627	0.06775	0.15381	0.03719	0.09251	0.25584	0.16623	0.26181	0.05985	0.10762	0.02192	0.00000	0.10747	0.03896
ZKB-7	2.34966	0.99711	0.07213	0.36965	0.44968	0.35391	0.69956	2.36119	0.49436	0.14159	0.38462	0.05262	0.09972	0.13603	0.03422
ZKB-7	2.08982	0.41274	0.06565	0.91076	0.04905	3.89576	0.00000	3.88549	0.41696	0.34719	0.26228	0.01820	0.05011	0.08471	0.03073
ZKB-7	2.46401	0.90508	0.21494	1.61647	0.01353	1.44007	0.02959	16.40996	0.65749	0.02853	0.02457	0.01513	0.15250	0.10288	0.02689
ZKB-7	<1.61973	0.26099	0.21254	0.84783	2.47576	58.78016	3.22862	12.91466	1.48526	0.20078	0.45606	0.14453	0.22386	0.08757	0.05614
ZKB-7	<1.42265	0.23492	0.07264	0.08365	0.05698	9.34577	0.06534	11.10711	0.15935	0.03004	0.04082	0.00849	0.04835	0.02565	0.02600
ZKB-7 aver	2.74652	0.95287	0.16654	0.57450	0.51370	14.76313	1.39467	6.19753	0.72105	0.13360	0.22035	0.05596	0.10551	0.03688	0.03422
ZKB-10	1.45789	2.90728	1.67098	0.39191	1.47158	2.93237	1.01223	15.26185	4.17645	0.76472	1.91687	0.20418	0.98754	0.17852	0.05556
ZKB-10	1.13165	1.82006	0.10263	0.31020	1.47215	0.11603	0.82474	30.40910	2.85213	0.95311	2.49383	0.36385	1.21648	0.16640	0.02617
ZKB-10	1.03435	1.68314	1.16246	0.82936	0.92394	0.17663	0.52051	4.06876	13.79940	0.33593	0.92941	0.23801	0.40089	0.19472	0.04057
ZKB-10	0.62983	3.12809	3.03119	1.58310	1.01171	0.46775	0.94808	0.97758	17.11457	0.61058	1.38673	0.23222	0.77161	0.27204	0.03611
ZKB-10	1.59975	0.84862	0.18905	0.22735	4.94641	0.18025	2.02176	0.27998	0.60947	1.23642	3.74377	0.51291	2.07068	0.53853	0.03335
ZKB-10	1.57801	2.04270	0.09942	0.03362	1.96161	0.22323	1.05715	16.97780	0.21781	0.90424	2.04175	0.28564	1.06412	0.41040	0.05913
ZKB-10	1.94790	2.54402	0.49506	0.84880	1.64365	0.15256	0.57798	0.17836	1.82914	0.50388	1.78909	0.27092	0.97661	0.17972	0.02549
ZKB-10	3.56835	2.55941	0.09058	0.07981	1.18631	0.16360	0.73463	17.53004	0.25600	0.45215	1.21093	0.12943	0.64401	0.14527	0.04033
ZKB-10	3.21489	4.06861	0.10503	0.04484	1.84470	0.10169	0.76938	14.28744	0.35320	1.12902	2.17092	0.30051	0.89572	0.18691	0.03329
ZKB-10	2.43418	4.44056	0.22263	0.25002	2.28526	0.28622	1.11857	5.94857	9.29467	2.14974	5.02067	0.69221	2.19475	0.37431	0.02224
ZKB-10	3.44304	3.57223	0.15901	0.14651	1.47584	0.28636	0.58666	2.99569	0.46160	1.33050	3.42254	0.44227	2.02228	0.22222	0.06036
ZKB-10 aver	2.14100	2.69225	0.87238	0.51343	1.83847	0.58817	0.92470	10.87368	4.63313	0.94275	2.37514	0.33383	1.20406	0.27560	0.02224
ZKB-11	1.29032	0.93022	0.03880	0.05913	0.80547	0.10263	0.33456	0.52884	0.04246	0.03329	0.16222	0.03056	0.07730	0.09173	0.04073
ZKB-11	1.07062	1.23766	0.07011	0.01321	0.83897	0.15548	0.45804	0.74395	0.16913	0.03056	0.06196	0.01104	0.06558	0.15634	0.02163
ZKB-11	1.67980	1.94407	0.07386	0.17033	1.14426	0.57278	0.66976	14.58998	0.37233	0.91208	2.54113	0.40923	1.23597	0.27748	0.01648
ZKB-11	1.90001	3.41637	0.12518	0.32072	0.85242	0.35648	0.58101	7.22066	0.50467	0.26093	0.85937	0.11918	0.46673	0.13040	0.02302
ZKB-11	1.51049	7.51870	1.15277	1.04354	0.95567	0.20134	0.37595	15.73222	3.71559	0.60326	1.73201	0.18967	0.61318	0.12892	0.02685
ZKB-11	2.85275	1.11216	0.05016	0.03755	0.44098	0.10248	0.15519	4.67028	0.21803	0.12367	0.36136	0.04913	0.22118	0.14121	0.03845
ZKB-11	2.57751	0.72630	0.05625	0.03791	0.57273	0.08517	0.33721	0.28968	0.13458	0.02193	0.22746	0.01710	0.10279	0.15923	0.02332
ZKB-11	<1.82568	2.36309	0.85643	0.38613	0.22102	0.15912	0.12899	1.64884	2.24634	0.08566	0.23405	0.03011	0.12269	0.14169	0.03718
ZKB-11	2.04522	0.51920	0.08871	0.03709	0.62083	0.09706	0.40483	1.51849	0.15656	0.02590	0.01849	0.01529	0.08881	0.10158	0.02615
ZKB-11 aver	1.86584	2.40607	0.55206	0.33218	0.71693	0.32152	0.38284	5.21588	1.37628	0.29278	0.77244	0.11792	0.63426	0.20394	0.02302

(continued on next page)

Table 5 (*continued*)

Sample	MgO	Al_2O_3	SiO_2	P_2O_5	CaO	Sc	TiO_2	V	Cr	MnO	Co	Ni	Cu	Zn	Ga
	wt%	wt%	wt%	wt%	wt%	ppm	wt%	ppm	ppm	wt%	ppm	ppm	ppm	ppm	ppm
Sample	Gd	Tb	Dy	Ho	Er	Tm	Yb	Lu	Hf	Ta	Re	Au	Pb	Th	U
	ppm	ppm	ppm	ppm	ppm	ppm	ppm	ppm	ppm	ppm	ppm	ppm	ppm	ppm	ppm
ZKB-7	0.30492	0.04718	0.10387	0.00703	0.08402	0.02472	0.11874	0.05226	0.12123	0.02973	0.00598	0.26304	0.09420	0.06370	0.02889
ZKB-7	0.23881	0.02168	0.08524	0.02604	0.02739	0.02583	0.00000	0.00000	0.00000	0.05587	0.00262	0.06253	0.05663	0.01909	0.01690
ZKB-7	0.09519	0.01496	0.05924	0.00000	0.04653	0.01380	0.06686	0.00830	0.06854	0.06186	0.00247	0.14339	0.29507	0.05116	0.03235
ZKB-7	0.07047	0.01371	0.14147	0.01888	0.05110	0.01746	0.06131	0.01596	0.04642	0.08103	0.00492	0.09533	1.42012	0.05028	0.03267
ZKB-7	0.10561	0.01582	0.04610	0.01156	0.03516	0.01499	0.05137	0.02458	0.26731	0.01279	0.00312	0.10844	0.28586	0.01932	1.47794
ZKB-7	0.12674	0.01376	0.05565	0.01891	0.04181	0.00771	0.08438	0.01653	0.20582	0.01545	0.00228	0.05427	3.62945	0.02378	0.01555
ZKB-7	0.20299	0.02172	0.21504	0.07671	0.54179	0.15963	1.36492	0.23411	1.95886	0.22251	0.00290	0.14322	3.62055	0.04689	0.32222
ZKB-7	0.10239	0.02616	0.09673	0.01437	0.04285	0.01379	0.07209	0.03562	0.79734	0.02150	0.00190	0.15524	0.05471	0.01942	0.02435
ZKB-7 aver	0.08283	#DIV/0!	0.15108	0.04187	0.20676	0.06402	0.71850	0.07565	0.80733	0.09020	0.00190	0.05840	1.85021	0.04032	0.60968
ZKB-10	0.23793	0.02859	0.30027	0.03019	0.12529	0.03389	0.29575	0.03045	0.13344	0.02598	0.00418	0.32688	28.45937	0.14929	0.21384
ZKB-10	0.36873	0.02984	0.18504	0.05861	0.30733	0.03790	0.26570	0.05506	0.06498	0.01615	0.00305	0.24574	4.04271	0.20942	0.43017
ZKB-10	0.09544	0.01836	0.24469	0.03094	0.14241	0.01469	0.11088	0.02542	0.06178	0.03250	0.00079	0.19763	8.61396	0.06918	0.14880
ZKB-10	0.24949	0.02666	0.15703	0.02915	0.08178	0.02051	0.26037	0.04084	0.13747	0.11082	0.00308	0.12715	16.59205	0.02103	0.05687
ZKB-10	0.58545	0.04544	0.58297	0.14246	0.59416	0.11322	0.68470	0.14458	0.00000	0.05250	0.00311	0.14618	2.17769	0.33318	0.43595
ZKB-10	0.25904	0.03364	0.27675	0.05546	0.20755	0.04303	0.48334	0.03920	0.05731	0.04377	0.00408	0.19314	0.44276	0.03441	0.41298
ZKB-10	0.13680	0.05191	0.24490	0.05330	0.14068	0.03513	0.36635	0.04732	0.06938	0.01389	0.00275	0.17536	4.97406	0.15186	0.30779
ZKB-10	0.24021	0.01577	0.14453	0.05094	0.17463	0.04126	0.19947	0.03778	0.10660	0.05125	0.00311	0.04770	0.35407	0.04003	0.25043
ZKB-10	0.18539	0.01797	0.33226	0.03685	0.33979	0.04204	0.22160	0.02677	0.00000	0.05182	0.00406	0.38037	1.89256	0.03549	0.40106
ZKB-10	0.31223	0.04685	0.24354	0.02548	0.38380	0.04315	0.46148	0.07133	0.06018	0.04112	0.00212	0.17978	7.04124	0.52286	0.39228
ZKB-10	0.21517	0.05185	0.08088	0.08691	0.15474	0.02652	0.19338	0.06420	0.06553	0.02278	0.00491	0.26950	3.65391	0.27719	0.28027
ZKB-10 aver	0.28361	0.03356	0.25390	0.06010	0.24111	0.04103	0.33496	0.06608	0.09342	0.05505	0.00330	0.09694	7.11313	0.21913	0.30277
ZKB-11	0.17375	0.02073	0.10692	0.03064	0.13029	0.03620	0.26159	0.03059	0.13652	0.02840	0.00141	0.60576	0.07600	0.02929	0.24823
ZKB-11	0.10451	0.03399	0.14719	0.01678	0.10702	0.01747	0.10849	0.03274	0.03595	0.02775	0.00259	0.81690	0.06447	0.03767	0.29591
ZKB-11	0.12664	0.04447	0.14461	0.03481	0.15889	0.03451	0.12790	0.01956	0.05800	0.01650	0.00165	0.54424	2.27624	0.12642	0.31176
ZKB-11	0.11223	0.01921	0.09108	0.01652	0.12491	0.01343	0.12710	0.01108	0.05606	0.00987	0.00164	0.50433	4.26785	0.05073	0.11550
ZKB-11	0.11059	0.02635	0.11369	0.02893	0.06042	0.02573	0.05676	0.01734	0.04247	0.01380	0.00140	<1.09143	14.25438	0.04786	0.26221
ZKB-11	0.17358	0.01509	0.06713	0.04163	0.05934	0.01705	0.12246	0.01984	0.04640	0.02138	0.00246	<1.02795	0.94847	0.02417	0.12750
ZKB-11	0.13672	0.01755	0.14276	0.02407	0.04949	0.01564	0.17729	0.03662	0.03932	0.01722	0.00210	0.44352	0.07975	0.01440	0.14172
ZKB-11	0.20456	0.01674	0.07964	0.01478	0.08344	0.03107	0.12162	0.00838	0.03872	0.02612	0.00169	0.34410	2.89282	0.01700	0.05656
ZKB-11	0.18545	0.03244	0.12807	0.05915	0.13765	0.02234	0.17854	0.02222	0.06299	0.06421	0.00206	0.53914	0.10524	0.03832	0.28492
ZKB-11 aver	0.10837	0.02815	0.11417	0.03013	0.11451	0.02208	0.15762	0.02027	0.08762	0.04072	0.00169	0.34410	4.92795	0.06229	0.20492

5. Sampling and analytical methods

Samples were collected from the skarn (in both outcrops and drill cores) at the 7918- and 7910 deposits (Fig. 2). The skarn-altered volcanic rock samples KD and KC in the outcrops, and seven skarn samples were collected for electron microprobe analysis (EMPA) (Fig. 2). The ore samples ZKB-7, ZKB-8 and ZKB-10 were collected for magnetite trace element analysis (Fig. 2).

Major oxide content analysis of garnet, pyroxene, amphibole, epidote and magnetite was performed with an EPMA-1600 electron microprobe at the State Key Laboratory of Isotope Geochemistry of the Guangzhou Institute of Geochemistry, Chinese Academy of Sciences (GIGCAS). Operation conditions included: Acceleration voltage of 15 kV, beam current of 18 nA and beam diameter of 1 μm. Vanadium concentration was corrected by analyzing V-free and Ti-bearing standards of rutile and native Ti because of the overlap between Ti Kβ and V Kα peaks (Carmichael, 1966). Precision of major and trace elements was better than 2% and 5%, respectively. Matrix corrections were performed by the ZAF procedures (Jurek and Hulínský, 1980). The molecular formula of amphibole is calculated with GeoKit-2013 (Lu, 2004).

Magnetite trace elemen analysis was performed at the State Key Laboratory of Isotope Geochemistry (GIGCAS) with a pulsed Resonetic 193 nm Laser Ablation (LA) system coupled with an Agilent 7500a ICP-MS. Helium was used as a carrier gas, and argon was used as the makeup gas and mixed with the carrier gas via a T–connector before entering the ICP. Each analysis incorporates a background acquisition of about 20 s (gas blank), followed by 40 s data acquisition for the sample. Analytical spots (23 μm) were ablated by 160 successive laser pulses (4 Hz). Element contents were calibrated against multiple reference materials (KL2-G and ML3B-G) using ^{57}Fe as the internal standard (Liu et al., 2008). KL2-G was analyzed for every five samples to correct the time-dependent drift of sensitivity and mass discrimination. Off-line selection and integration of background and analytical signals, time drift correction and quantitative calibration were performed by ICPMS Data Cal8.3 (Liu et al., 2008). Detailed operating conditions for the LA system and the ICP-MS instrument and data reduction were similar to those described by Liu et al. (2008).

6. Results

6.1. Skarn mineralogy

Compositions of the Kaladawan pyroxene, garnet, amphibole and epidote were listed in Tables 1, 2, 3 and 4, respectively. The pyroxene has variable FeO_T and MgO contents ranging 1.22–13.73 wt.% and 9.45–17.21 wt.%. Pyroxene is dominated by diopside (55.4–94.7 mol%) and hedenbergite (42.5–4.7 mol%) (Fig. 5A, Table 1). The two types of garnet (*Type 1* and *Type 2*) did not exhibit distinct chemical differences (Fig. 5B, Table 2), with the major element contents being SiO_2 = 34.01–36.67 wt.%, Al_2O_3 = 0–8.41 wt.%, FeO_T = 19.11–28.48 wt.% and CaO = 34.76–36.10 wt.%. The garnet is dominated by andradite (61.2–94.4 mol%), followed by grossularite (37.5–5.0 mol%). Discernible compositional change from core to rim is absent (Fig. 6A, B). The amphibole contains SiO_2, CaO, MgO, FeO_T and Al_2O_3 contents of 53.60–59.06 wt.%, 13.49–25.58 wt.%, 15.48–23.78 wt.%, 1.66–12.90 wt.% and 0.02–3.84 wt.%, respectively (Table 3). All the amphibole is calcic and dominated by tremolite and actinolite (Fig. 7).

The Kaladawan epidote contains SiO_2 = 36.79–38.67 wt.%, Al_2O_3 = 21.80–28.42 wt.%, FeO_T = 5.42–14.08 wt.%, MgO = 0.01–0.05 wt.%,

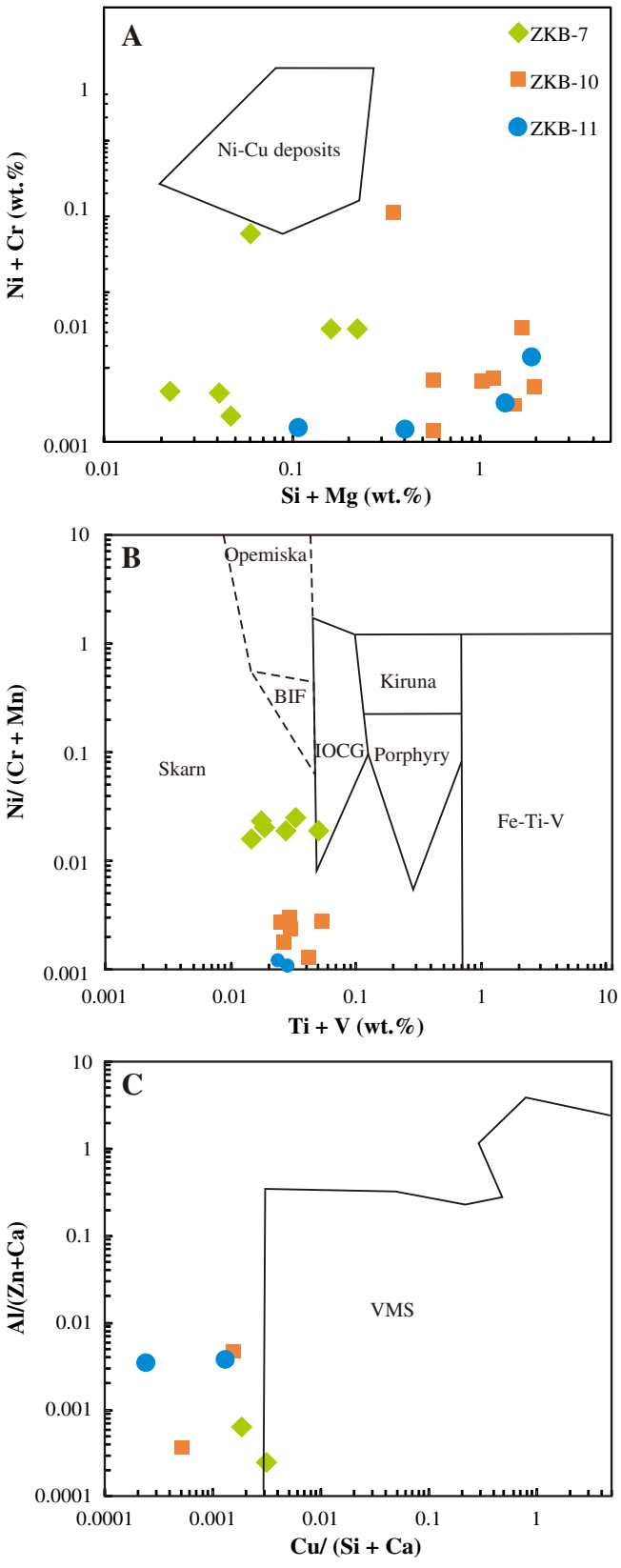

Fig. 8. Provenance discrimination diagram of the Kaladawan magnetite. (A) (Si + Mg) vs. (Ni + Cr) (Dupuis and Beaudoin, 2011). (B) Ni/(Cr + Mn) vs. (Ti + V) (Nadoll et al., 2014a). (C) Cu/(Si + Ca) vs. Al/(Zn + Ca) (Dupuis and Beaudoin, 2011).

CaO = 24.17–25.50 wt.%, and Al_2O_3 = 0.03–0.52 wt.%, respectively (Table 4). The epidote group minerals include mainly epidote with minor zoisite.

6.2. Magnetite trace element geochemistry

The Kaladawan magnetite contains relatively hign Mg (Table 5), whereas Ca, Si, Al are lower than those of in typical Fe skarn magnetite (Dare et al., 2014). The magnetite has variable Cr contents (from below detection limits to >800 ppm). The Mo, Ba, Pb and Zr contents range from <1 ppm to >10 ppm. Trace elements, such as Sc, Rb, Sr, Nb, Ta, Hf, REEs, Th and U concentrations, are generally below 1 ppm.

7. Discussion

7.1. Skarn formation

Skarns are rocks dominated by Ca-silicate minerals (e.g., garnet and diopside), and extensively developed in both skarn- and SVIO-type Fe deposits. Different genetic models were proposed for the skarn in these two deposit types. Skarn in typical skarn Fe deposits is generally regarded to be formed by contact metamorphic/metasomatic processes involving magmatic and/or meteroic fluids (Chen et al., 2007; Deng et al., 2017; Meinert et al., 2005; Pirajno, 2009; Yang et al., 2013), whereas that in SVIO-type Fe deposits may have formed by the reaction between submarine-volcanism-related hydrothermal fluids and seafloor rocks, as proposed by the syngenetic volcanic exhalation–sedimentation model (Hou et al., 2014b; Jiang and Wang, 2005). The composition of skarn minerals could reflect the physical and chemical conditions under which they formed, thus, could be used to constrain the genesis of the skarn. For the case of the Kaladawan Fe–Mo ore field, we suggest that a skarn-type origin is more appropriate because:

(1) Skarn is subdivided into calcic-, magnesian- and manganoan skarns (Einaudi et al., 1981; Korzhinskiy, 1964; Meinert et al., 2005; Zhao et al., 2003). The Ca-bearing silicate mineral assemblages (grossular–andradite series, diopside–hedenbergite series, tremolite–actinolite series and epidote) and marble host rocks indicate that the Kaladawan skarn is calcic, resembling many skarn-type Fe deposits (Meinert et al., 2005). (2) The Kaladawan skarn mineral chemistry resembles those of typical skarn Fe deposits: (i) The Kaladawan pyroxene contains more diopside (55.5–94.7 mol%) than hedenbergite (Hd: 42.6–4.7 mol%), similar to typical skarn-type Fe and Mo deposits worldwide (Fig. 5A). (ii) Garnet from typical skarn-type Fe deposits is generally dominated by andradite with minor grossular (Einaudi et al., 1981; Meinert et al., 2005), whereas that garnet from typical volcanic exhalative sedimentation deposits (including SVIO-type deposits) is featured by Mn- and Fe-rich spessartine and almandine due to Fe–Mn enrichment on the seafloor (Burton et al., 1999; Hou et al., 2014b). The Kaladawan garnet is dominated by andradite (Adr: 61.2–94.4 mol%) and grossularite (Grs: 37.5–5.0 mol%), similar to typical skarn-type Fe and Mo deposits worldwide (Fig. 5B). (iii) EMPA results indicate that the magnetite-associated amphibole from Kaladawan is dominated by actinolite (Fig. 7), similar to those of typical skarn-type Fe deposits (Fe-rich in the tremolite–actinolite series; Meinert et al., 2005).

In summary, the Kaladawan skarn resembles that of in typical skarn-type Fe–Mo deposits in terms of its mineral assemblage, composition and spatial relationship with intrusion, and should be formed by contact metasomatism of the granite-derived fluids with marble.

7.2. Genesis of the Kaladawan Fe–Mo ore field

Various genetic models have been proposed to explain the origin of the Kaladawan Fe–Mo ore field: hydrothermal metasomatic-filling (Qi et al., 2008), synsedimentary–exhalative (SEDEX) with later hydrothermal overprint (Chen et al., 2009, 2012; Gao et al., 2012; Hao, 2013) and SVIO-type (Hou et al., 2014a). Magnetite geochemistry is a useful petrogenetic and provenance indicator to discriminate magnetite from the various source rocks and mineral deposit types (Dare et al., 2014; Dupuis and Beaudoin, 2011; Hu et al., 2015; Huang et al., 2015; Nadoll et al., 2014a). The magnetite crystallized from the gabbro- and

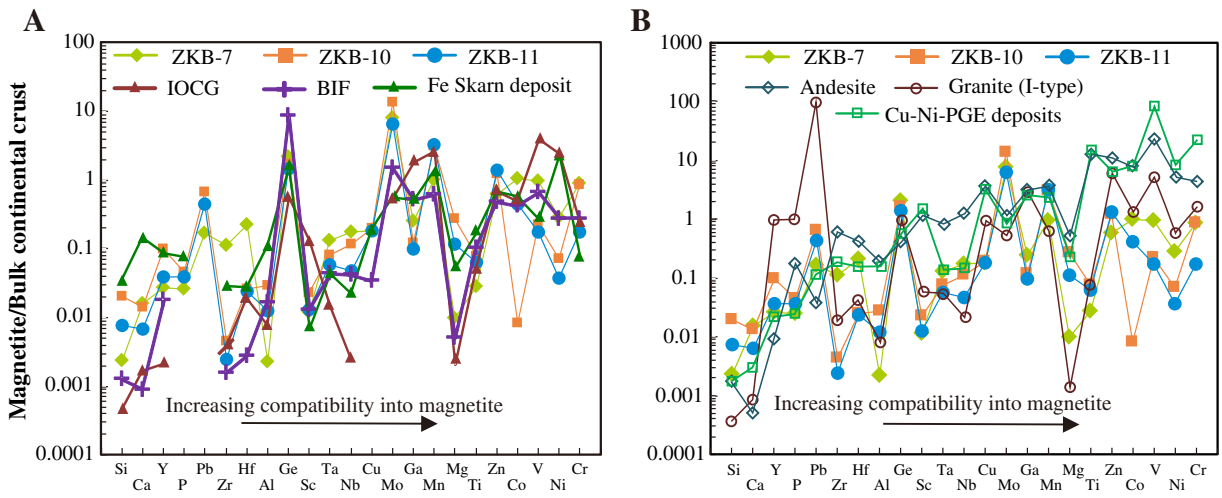

Fig. 9. Multi-element diagrams of average trace element concentrations in magnetite normalized to the bulk continental crust (normalization values from Rudnick and Gao, 2003). Magnetite from (A) IOCG, BIF and Fe skarn deposit and (B) Granite, andesite and Cu-Ni-PGE deposit are shown for comparison. Data for IOCG, BIF, Fe skarn deposit, granite, andesite and Cu-Ni-PGE deposit are from Dare et al. (2014). Data for IOCG deposits are from Potvin-Doucet (2012) and Dare et al. (2014).

dolerite-derived fluids may be similar to that from magmatic Ni-Cu-PGEs deposits (characterized by high contents of Ti, V, Cr and Ni, Dare et al., 2014). However, the low Ti, Cr and Ni contents of the Kaladawan magnetite indicate a hydrothermal (rather than magmatic) origin (Dare et al., 2014; Dupuis and Beaudoin, 2011). It is also supported by that the Kaladawan magnetite data points were plotted outside the Ni-Cu deposits field (Fig. 8A) but inside the skarn field (Fig. 8B), reaffirming its skarn origin and precluding a sedimentary-related (e.g., BIFs, SEDEX) origin. The geochemical data for magnetite from SVIO-type deposits are rarely published. Nevertheless, the magnetite from submarine volcanic rocks, VMS and Fe–Mn oxide (concretion) deposits can be served as a proxy to the SVIO-derived magnetite, as the fact that SVIO deposits are formed by submarine magmatism and related post-magmatic hydrothermal activities (Hou et al., 2014a; Jiang and Wang, 2005). Magnetite from VMS deposits, typically contains high Si, Zn and Ca and low Al (Dupuis and Beaudoin, 2011), is markedly different from the Kaladawan magnetite. Similarly, in the discrimination diagram, all the Kaladawan magnetite data points were plotted outside the VMS field (Fig. 8C). In addition, the Kaladawan magnetite has bulk continental crust-normalized multi-element patterns similar to that of the Vegas Peledas skarn Fe deposit (Fig. 9A; Pons et al., 2009), but distincts from magnetite of igneous rocks (e.g., andesite and granite), BIFs and magmatic Cu-Ni-PGEs deposits (Fig. 9B).

Furthermore, the Kaladawan Fe–Mo ore field share similar characters to typical skarn deposits, e.g., the Yangtze River Valley metallogenic belt (Mao et al., 2011; Pan and Dong, 1999; Zhai et al., 1996), the Shangfanggou Mo–Fe deposit in Eastern Qinling (Yang et al., 2013), the Xiaobaishitou W (–Mo) deposit in eastern Tianshan (Deng et al., 2017) and the Vegas Peledas skarn Fe deposit in Argentina (Pons et al., 2009). These characters include: (1) The orebodies occur in the contact zones with the host rocks; (2) Skarns are extensively developed and formed by the interaction between fluids derived from intrusions and host rocks; (3) metallogenesis is spatially associated with skarn alteration. Therefore, the Kaladawan ore field is a skarn system.

7.3. Implications for Mo mineralization

The Kaladawan molybdenite grains were Re–Os dated to be 477.1 ± 7.0 Ma to 483.3 ± 7.0 Ma (Hao, 2013). These ages were younger than the Cambrian host rocks but consistent with that of the 476.1 ± 3.6 Ma Kaladawan intrusions (Wang et al., 2016), which indicated that the Mo mineralization was associated with the intrusions. The Kaladawan magnetite has higher Mo concentration (up to 30 ppm, median = 5 ppm, Table 5) than those of many skarn Fe deposits in the world, which commonly have Mo concentration below the detection limits (Fig. 9A; Nadoll et al., 2014a, 2014b; Zhao and Zhou, 2015). Molybdenite occurs as veinlets crosscutting magnetite ores and associated with other sulfide minerals (pyrite + chalcopyrite + pyrrhotite + sphalerite + galena) at the Kaladawan, suggesting a later formation (Fig. 3F, G). In fact, the assemblage was well match up that of sulfide mineralization stage in skarn-type deposits, which further confirmed that the Kaladawan Fe–Mo mineralization is skarn-type. As indicated by the high resolution SEM imaging, the high Mo concentration in the Kaladawan magnetite is not caused by molybdenite inclusions (as they are absent). Instead, the Mo may have been introduced directly from the Mo-rich hydrothermal fluids into the magnetite crystal lattices.

8. Conclusions

(1). The Kaladawan Fe (–Mo) deposits are hosted in the skarn-altered Upper Cambrian Tashibulake Formation marble and volcanic–sedimentary sequences. The orebodies are distributed in the skarn in contact with the Kaladawan granite, similar to typical skarn system.

(2). The Kaladawan ore-hosting skarn comprises garnet (61.2–94.4 mol% andradite; 37.5–5.0 mol% grossularite) and pyroxene (55.4–94.7 mol% diopside; 42.5–4.7 mol% hedenbergite), resembling typical skarn Fe and Mo deposits worldwide. The Kaladawan skarn were formed by contact metasomatism between the granite-derived fluids and the Tashibulake Formation volcanic–sedimentary rocks.

(3). The Kaladawan magnetite has unusually high Mg, Mo and Cr contents, and its (Ti + V) and (Al + Mn) values are similar to typical skarn Fe mineralization but distinct from SVIO-type mineralization.

(4). The Kaladawan Fe–Mo ore field is a skarn system.

Acknowledgements

This research was funded by the Chinese National Basic Research 973-Program (2014CB440802), NSFC (41672086, 41402061, 41072077), Geological Survey of China (1212011140056) and the CAS Knowledge Innovation Program (40730421). The authors thank the engineers of No. 1 Geological Team of the Xinjiang Geological Survey, especially thank Wan-Xiu Qi and Bing Liu for their field support. We

are grateful to Cong-Ying Li, Kun Wang, Lin-Li Chen, Pin Wang, Wei-Feng Zhang and Lian-Dang Zhao for helping with the geochemical analyses and valuable dissussions. Constructive suggestions, pertinent comments and careful corrections by two anonymous reviewers and Prof. Franco Pirajno, as well as guest editor Dr. Xiao-Hua Deng greatly improved the quality of the manuscript. Cenozoic Geoscience Editing is acknowledged for its scientific and language editing service.

References

Burton, K.W., Bourdon, B., Birck, J.L., Allègre, C.J., Hein, J.R., 1999. Osmium isotope variations in the oceans recorded by Fe–Mn crusts. Earth Planet. Sci. Lett. 171, 185–197.

Carmichael, I.E., 1966. The iron-titanium oxides of salic volcanic rocks and their associated ferromagnesian silicates. Contrib. Mineral. Petrol. 14, 36–64.

Chen, X., Yin, A., Gehrels, G.E., Cowgill, E.S., Grove, M., Harrison, T.M., Wang, X.F., 2003. Two phases of Mesozoic north-south extension in the eastern Altyn Tagh range, northern Tibetan Plateau. Tectonics 22, 8-1–8-22. http://dx.doi.org/10.1029/2001TC001336.

Chen, Y.J., Chen, H.Y., Zaw, K., Pirajno, F., Zhang, Z.J., 2007. Geodynamic settings and tectonic model of skarn gold deposits in China: an overview. Ore Geol. Rev. 31, 139–169.

Chen, B., Jiang, R., Li, L., Chen, Z., Qi, W., Liu, R., Cui, L., Wang, S., 2009. Discovery of iron ore zone in the Kaladawan area within the eastern part of the Altun Mountains and its significance. Acta Geosci. Sin. 30, 143–154 in Chinese with English abstract.

Chen, Y., Dai, J.Y., Li, G., An, L.X., 2012. The geological characteristics of Kaladawan iron deposit and its prospecting criterias. Xinjiang Nonferrous Met. 1, 1–3 in Chinese.

Cui, L., Chen, B., Yong, N., Chen, Z., Ding, W., 2010. Geochemistry and genesis of basic–intermediate volcanic rocks from Kaladawan, east Altun taugh mountain. J. Geomech. 16, 96–107 in Chinese with English abstract.

Dare, S.A.S., Barnes, S.J., Beaudoin, G., Méric, J., Boutroy, E., Potvin-Doucet, C., 2014. Trace elements in magnetite as petrogenetic indicators. Mineral. Deposita 49, 785–796.

Deng, X.H., Chen, Y.J., Santosh, M., Wang, J.B., Li, C., Yue, S.W., Zheng, Z., Chen, H.J., Tang, H.S., Dong, L.H., Qu, X., 2017. U–Pb zircon, Re–Os molybdenite geochronology and Rb-Sr geochemistry from the Xiaobaishitou W (−Mo) deposit: implications for Triassic tectonic setting in eastern Tianshan, NW China. Ore Geol. Rev. 80, 332–351.

Dupuis, C., Beaudoin, G., 2011. Discriminant diagrams for iron oxide trace element fingerprinting of mineral deposit types. Mineral. Deposita 46, 319–335.

Einaudi, M.T., Meinert, L.D., Newberry, R.T., 1981. Skarn deposits. Econ. Geol. 317–391 (75th Anniv.).

Ettlinger, A.D., 1990. A Geological Analysis of Gold Skarns and Precious Metal Enriched Iron and Copper Skarns in British Columbia, Canada (Ph.D. Thesis). Washington State University, Washington.

Gao, X.F., Xiao, P.X., Kang, L., Guo, L., Dong, Z.C., Xi, R.G., 2012. The origin of volcanic rocks in the Kaladawan iron ore district of eastern Altun Mountains and its geological and metallogenic significance. Geol. Bull. China 31, 2070–2075 in Chinese with English abstract.

Hao, R.X., 2013. The Characteristics and Genetic of Kaladawan Area Iron Deposit, Altyn Tagh, Xinjiang (Master Thesis). Chinese Academy of Geological Sciences, Beijing, pp. 1–89 in Chinese with English abstract.

He, G.Q., Chen, S.D., Xu, X., Li, J.Y., Hao, J., Li, X.Y., Zhao, J., Zheng, L.X., Li, Y., 2005. An introduction to the explanatory text of the map of tectonics of Xinjiang and its neighbouring area 1: 1500000. Geological Publishing House, Beijing (in Chinese).

Hou, T., Zhang, Z., Pirajno, F., Santosh, M., Encarnacion, J., Liu, J., Zhao, Z., Zhang, L., 2014a. Geology, tectonic settings and iron ore metallogenesis associated with submarine volcanism in China: an overview. Ore Geol. Rev. 57, 498–517.

Hou, T., Zhang, Z.C., Santosh, M., Encarnacion, J., Zhu, J., Luo, W.J., 2014b. Geochronology and geochemistry of submarine volcanic rocks in the Yamansu iron deposit, eastern Tianshan Mountains, NW China: Constraints on the metallogenesis. Ore Geol. Rev. 56, 487–502.

Hu, H., Lentz, D., Li, J.W., McCarron, T., Zhao, X.F., Hall, D., 2015. Reequilibration processes in magnetite from iron skarn deposits. Econ. Geol. 110, 1–8.

Huang, X.W., Gao, J.F., Qi, L., Zhou, M.F., 2015. In-situ LA-ICP-MS trace elemental analyses of magnetite and Re–Os dating of pyrite: the Tianhu hydrothermally remobilized sedimentary Fe deposit, NW China. Ore Geol. Rev. 65, 900–916.

Jiang, F.Z., Wang, Y.W., 2005. Marine Volcanic Rocks and Related Metallic Ore Deposits. Metallurgical Industry Press, Beijing (248 pp). in Chinese.

Jurek, K., Hulínský, V., 1980. The use and accuracy of the ZAF correction procedure for the microanalysis of glasses. Microchim. Acta 73, 183–198.

Korzhinskiy, D.S., 1964. An outline of metasomatic process (part 2 of 3). Int. Geol. Rev. 6, 1920–1952.

Leake, B.E., Woolley, A.R., Birch, W.D., Burke, E.A.J., Ferraris, G., Grice, J.D., Hawthorne, F.C., Kisch, H.J., Krivovichev, V.G., Schumacher, J.C., Stephenson, N.C.N., Whittaker, E.J.W., 2004. Nomenclature of amphiboles: additions and revisions to the International Mineralogical Association's amphibole nomenclature. Eur. J. Mineral. 89, 191–196. http://dx.doi.org/10.1127/0935-1221/2004/0016-0191.

Li, N., Ulrich, T., Chen, Y.J., Thompson, T.B., Pease, V., Pirajno, F., 2012. Fluid evolution of the Yuchiling porphyry Mo deposit, East Qinling, China. Ore Geol. Rev. 48, 442–459.

Liu, Y., Hu, Z., Gao, S., Günther, D., Xu, J., Gao, C., Chen, H., 2008. In situ analysis of major and trace elements of anhydrous minerals by LA-ICP-MS without applying an internal standard. Chem. Geol. 257, 34–43.

Liu, Y.S., Yu, H.F., Xin, H.T., Lu, S.N., Xiu, Q.Y., Li, Q., 2009. Tectonic units division and Precambrian significant geological events in Altyn Tagh Mountain, China. Geol. Bull. China 28, 1430–1438 in Chinese with English abstract.

Lu, Y., 2004. GeoKit—A geochemical toolkit for Microsoft excel. Geochimica 33, 459–464 In Chinese with English abstract.

Mao, J., Xie, G., Duan, C., Pirajno, F., Ishiyama, D., Chen, Y., 2011. A tectono-genetic model for porphyry-skarn-stratabound Cu-Au-Mo-Fe and magnetite-apatite deposits along the Middle-Lower Yangtze River valley, Eastern China. Ore Geol. Rev. 43, 294–314.

Meinert, L.D., Dipple, G.M., Nicolescu, S., 2005. World skarn deposits. Econ. Geol. 299–336 (100th Anniv.).

Nadoll, P., Angerer, T., Mauk, J.L., French, D., Walshe, J., 2014a. The chemistry of hydrothermal magnetite: a review. Ore Geol. Rev. 61, 1–32.

Nadoll, P., Mauk, J.L., Leveille, R.A., Koenig, A.E., 2014b. Geochemistry of magnetite from porphyry Cu and skarn deposits in the southwestern United States. Mineral. Deposita 50, 493–515.

Pan, Y., Dong, P., 1999. The Lower Changjiang (Yangzi/Yangtze River) metallogenic belt, east Central China: intrusion- and wall rock-hosted Cu-Fe-Au, Mo, Zn, Pb, Ag deposits. Ore Geol. Rev. 15, 177–242.

Pirajno, F., 2009. Hydrothermal Processes and Mineral Systems. Springer, Berlin (1250 pp.).

Pons, J.M., Franchini, M., Meinert, L., Recio, C., Etcheverry, R., 2009. Iron skarns of the Vegas Peladas District, Mendoza, Argentina. Econ. Geol. 104, 157–184.

Potvin-Doucet, C., 2012. Distribution et comparaison d'éléments traces dans la magnétite contenue dans des granites de types I et S. Sciences de la terre. Université du Québec à Chicoutimi, Québec, pp. 1–43.

Qi, W.X., Ma, Y.Z., Wang, R., Wei, X.C., Jiang, J.Y., 2008. The geological characteristics of Baba iron deposit, northern margin area of Altyn Mountain and its criteria for prospecting and genesis. Xinjiang Geol. 26, 253–257 in Chinese with English abstract.

Ramdohr, P., 1926. Beobachtungen an Magnetit, Ilmenit, Eisenglanz, und Uberlegungeniiber das System FeO–Fe_2O_3–TiO2. Neues Jahrb. Mineral. 54A, 320–379.

Rudnick, R.L., Gao, S., 2003. Composition of the Continental Crust. In: Holland, H.D., Turekian, K.K. (Eds.), Treatise on Geochemistry. Elsevier-Pergaman, Oxford, pp. 1–64.

Sidder, G.B., 1985. Ore Genesis at the Monterrosas Deposit in the Coastal Batholith, Ica, Peru (Ph.D. Thesis). Oregon State University, Oregon, pp. 1–232.

Wang, C.M., Zhang, L., Chen, H.Y., Tang, H.S., Chen, Y.J., Dong, L.H., Qu, X., Zheng, Y., Li, D.F., Fang, J., 2016. Zircon U–Pb age, geochemistry and Sr–Nd–Hf isotopes of the ore-associated granites at the Kaladawan Fe–Mo ore field (Altyn), NW China. Ore Geol. Rev. (under review).

Xin, H.T., 2012. The Chronotectonic Framework and Main Geological Events of Early Precambrian in the Agetashtage area, Southeastern Margin of Tarim basin (Ph.D. Thesis). China University of Geosciences, Beijing, pp. 1–127 (in Chinese with English abstract).

Xin, H., Zhao, F., Luo, Z., Liu, Y., Wan, Y., Wang, S., 2011. Determination of the Paleoproterozoic geochronological framework in Aqtashtagh area in southeastern Tarim, China, and its geological significance. Acta Geol. Sin. 85, 1977–1993 in Chinese with English abstract.

Yang, J.S., Shi, D.R., Wu, C.L., Su, D.C., Chen, S.Y., Wang, X.B., Wooden, J., 2008. Petrology and SHRIMP age of the Hongliugou ophiolite at Milan, north Altun, at the northern margin of Tibetan plateau. Acta Petrol. Sin. 024, 1567–1584 in Chinese with English abstract.

Yang, Y., Chen, Y.J., Zhang, J., Zhang, C., 2013. Ore geology, fluid inclusions and four-stage hydrothermal mineralization of the Shangfanggou giant Mo–Fe deposit in eastern Qinling, Central China. Ore Geol. Rev. 55, 146–161.

Zhai, Y.S., Xiong, Y.L., Yao, S., Lin, X., 1996. Metallogeny of copper and iron deposits in the eastern Yangtse Craton, east-Central China. Ore Geol. Rev. 11, 229–248.

Zhang, Z., Hou, T., Santosh, M., Li, H., Li, J., Zhang, Z., Song, X., Wang, M., 2014. Spatio-temporal distribution and tectonic settings of the major iron deposits in China: an overview. Ore Geol. Rev. 57, 247–263.

Zhao, W.W., Zhou, M.F., 2015. In-situ LA–ICP-MS trace elemental analyses of magnetite: the Mesozoic Tengtie skarn Fe deposit in the Nanling Range, South China. Ore Geol. Rev. 65, 872–883.

Zhao, Y., Dong, Y., Li, D., Bi, C., 2003. Geology, mineralogy, geochemistry, and zonation of the Bajiazi dolostone-hosted Zn–Pb–Ag skarn deposit, Liaoning Province, China. Ore Geol. Rev. 23, 153–182.